Approximate analytic spectra of reionized CMB anisotropies and polarization generated by relic gravitational waves

T. Y. Xia and Y. Zhang*

Key Laboratory of Galactic and Cosmological Research, Astrophysics Center, The University of Sciences and Technology of China, Chinese Academy of Sciences, Hefei, Anhui, China

(Received 21 February 2009; published 9 April 2009)

We present an approximate, analytical calculation of the reionized spectra C_l^{XX} of cosmic microwave background radiation anisotropies and polarizations generated by relic gravitational waves (RGWs). Three simple models of reionization are explored, whose visibility functions are fitted by Gaussian types of functions as approximations. We have derived the analytical polarization β_l and temperature anisotropies α_l, which both consist of two terms proportional to RGWs at the decoupling and at the reionization as well. The explicit dependence of β_l and α_l upon the reionization time η_r, the duration $\Delta\eta_r$, and the optical depth κ_r is demonstrated. Moreover, β_l and α_l contain κ_r in different coefficients, and the polarization spectra C_l^{EE} and C_l^{BB} are more sensitive probes of reionization than C_l^{TT}. These results facilitate examination of the reionization effects, in particular, the degeneracies of κ_r with the normalization amplitude and with the initial spectral index of RGWs. It is also found that reionization causes a κ_r-dependent shift $\Delta l \sim 20$ of the zero multipole l_0 of C_l^{TE}, an effect that should be included in order to detect the traces of RGWs. Compared with numerical results, the analytical C_l^{XX} are approximate and have the limitation. For the primary peaks in the range $l \simeq (30, 600)$, the error is $\leq 3\%$ in three different models. In the range $l < 20$ for the reionization bumps, the error is $\leq 15\%$ for C_l^{EE} and C_l^{BB} in the two extended reionization models, and C_l^{TT} and C_l^{TE} have much larger departures for $l < 10$. The bumps in the sudden reionization model are too low.

DOI: 10.1103/PhysRevD.79.083002 PACS numbers: 98.70.Vc, 04.30.−w, 04.30.Nk, 98.80.−k

I. INTRODUCTION

Reionization is a very important cosmological process, which might be, to a large extent, determined by the first luminous objects formed in the early Universe, either star-forming galaxies or active galactic nuclei. Our knowledge of the cosmic structure formation of the Universe would be incomplete without a reliable account of reionization history, the details of which are still not understood yet. During the evolution history of CMB, the reionization taking place around the redshift $z = (6–20)$ is a major process in shaping the profiles of CMB spectra on large scales, only secondary to the decoupling around $z \sim 1100$. Reionization leaves observable prints on CMB [1–8] through the interaction between the CMB photons and the reionized free electrons. In particular, the spectra of CMB anisotropies and polarizations on large angular scales contain the distinguished signatures of reionization. Thereby, complementary to the constraints on the late stage of reionization $z \simeq 6$ from observations of the most distant quasar absorption lines, etc., CMB provides a unique probe for the early stage of reionization. On the other hand, in order to interpret the observed spectra of CMB anisotropies and polarizations within the standard model, the reionization-induced modifications have to be taken into account properly. As is known, the reionization parameters could be entangled with the cosmological parameters, thus biasing our interpretation of CMB, and of reionization as well [9–14]. In this regard, analytic studies can improve our understanding of CMB and reionization, even though comparisons with the observed data require more accurate numerical calculations, such as CMBFAST and CAMB [15,16].

Two kinds of perturbations of the spacetime metric, i.e., density perturbations [17–19] and relic gravitational waves (RGWs) [18,20–22], will effectively influence the CMB through the Sachs-Wolfe term [23] in the Boltzmann equation for photons. Although the contribution from density perturbations is dominant, RGWs give rise to a magnetic type of CMB polarizations, providing a distinguished channel to directly detect RGWs with very long wavelengths [9,11,24,25]. Moreover, RGWs give substantial contributions to the large angular scale part of CMB spectra, where the impact of reionization is also dominant and causes bumps in the CMB polarization spectra for $l < 10$. Thus, in order to study reionization through the CMB, one has to take into account the contribution of RGWs or vice versa.

Analyses have been made towards CMB anisotropies and polarizations generated by RGWs [20,21,25–31]. In particular, by an approximate treatment of the time integration over the decoupling process during the recombination, Refs. [32,33] have derived the analytic expressions of the CMB polarization spectra, C_l^{EE} and C_l^{BB}. Recently,

*yzh@ustc.edu.cn

extending the previous works, we have improved the time integration by a better approximation, and obtained the analytical expressions of the four spectra, including C_l^{TT} and C_l^{TE} [34], which agree fairly well with the numerical results up to a broader range of multipole moments, $l < 600$. In that work the damping on RGWs due to neutrino free-streaming (NFS) has been included [35–38], and its effects on the cross spectrum C_l^{TE} have been demonstrated in detail. In these analytical calculations, the reionization process has not been included, and will be addressed in this paper. For the purpose of calculating the reionized CMB spectra C_l^{XX}, the reionization can be treated similarly to the decoupling, if the visibility functions for both processes are given. While the decoupling and its visibility function $V_d(\eta)$ effectively distributed around $z \sim 1100$ have been better studied, the reionization is currently less understood, and is commonly modeled by its ionization fraction $X_e(\eta)$ as a function of time. We shall examine three possible simple reionization models with explicit $X_e(\eta)$, which, for a given value of the optical depth κ_r, can be converted into its corresponding visibility function $V_r(\eta)$ effectively distributed around $z \sim 11$. The functions $V_d(\eta)$ and $V_r(\eta)$ are separately distributed, not overlapping; each of them can, respectively, be approximated by Gaussian types of functions, which are specified by their location, height, and width. In parallel, we will carry out, with an approximation, the time integrations of Boltzmann's equation for the decoupling and reionization processes. The modes α_l and β_l, respectively, for CMB temperature anisotropies and polarization, are obtained as analytical expressions. Each mode explicitly consists of two separated parts, one from the decoupling and the other from the reionization. Moreover, the optical depth κ_r appears as the coefficients in α_l and β_l in different combinations, and probabilistic interpretations are given. Besides reionization and decoupling, the result also contains other cosmological parameters for inflation that are contained in RGWs. Thus analytic studies on the reionization effects will be facilitated.

In Sec. II we review briefly the result of the RGW spectrum $h(\nu, \eta)$ that will be used as the source for CMB anisotropies and polarization. In Sec. III three models of homogeneous reionization $X_e(\eta)$ are presented: one sudden and two extended. For each model the visibility function $V_r(\eta)$ and the optical depth function $\kappa_r(\eta)$ are presented. In Sec. IV, by approximately carrying out the time integrations, the analytical expressions of α_l and β_l are obtained. The resulting spectra C_l^{XX} are demonstrated. In Sec. V, detailed analyses are made towards the reionization effects upon C_l^{XX}, three models are compared, and, in particular, examinations are made on the degeneracies of κ_r with the normalization amplitude A and the initial spectral index $\beta_{\rm inf}$ of RGWs produced during inflation. The effect of reionization on the zero-multipole analysis is addressed. The conclusion is given in Sec. VI. We use the units in which $c = \hbar = k_B = 1$ in this paper.

II. RGWS SPECTRUM

The expansion of a spatially flat universe can be described by the spatially flat ($\Omega_\Lambda + \Omega_m + \Omega_r = 1$) Robertson-Walker spacetime with a metric

$$ds^2 = a^2(\eta)[-d\eta^2 + (\delta_{ij} + h_{ij})dx^i dx^j], \tag{1}$$

where $a(\eta)$ is the scale factor, η is the conformal time, and h_{ij} are the gravitational waves, taken to be traceless and transverse (TT gauge), $h^i{}_i = 0$ and $h_{ij,j} = 0$. By the Fourier decomposition

$$h_{ij}(\eta, \mathbf{x}) = \sum_\sigma \int \frac{d^3k}{(2\pi)^3} \epsilon_{ij}^\sigma h_{\mathbf{k}}^{(\sigma)}(\eta) e^{i\mathbf{k}\cdot\mathbf{x}} \tag{2}$$

for each mode $\mathbf{k}$ and each polarization $\sigma = (+, \times)$, the wave equation takes the form

$$\ddot{h}_k + 2\frac{\dot{a}}{a}\dot{h}_k + k^2 h_k = 0, \tag{3}$$

where the polarization index σ has been skipped for simplicity, and the subindex $\mathbf{k}$ can be replace by k since the perturbations are assumed to be isotropic. The analytic solution of Eq. (3) has been given for the expanding Universe with consecutive stages: inflationary, reheating, radiation-dominant, matter-dominant, and accelerating, respectively, in Refs. [38–40]. In our convention,

$$a(\eta) = a_m(\eta - \eta_m)^2, \qquad \eta_2 \le \eta \le \eta_E, \tag{4}$$

for the matter-dominant stage, and

$$a(\eta) = l_H|\eta - \eta_a|^{-\gamma}, \qquad \eta_E \le \eta \le \eta_0, \tag{5}$$

for the accelerating stage up to the present time η_0, where $\gamma \simeq 1.044$ for $\Omega_\Lambda = 0.75$, and $l_H = \gamma/H_0$, H_0 is the Hubble constant. The normalization of $a(\eta)$ is chosen to be $|\eta_0 - \eta_a| = \eta_a - \eta_0 = 1$, where we have taken $\eta_0 = 3.11$ to be the present time. Then, once the ratio Ω_Λ/Ω_m is specified, all the parameters will be fixed: $a_m = l_H \frac{\gamma^2}{4} \zeta_E^{-(1+2/\gamma)}$, $\eta_E = \eta_a - \zeta_E^{1/\gamma}$, $\eta_m = \eta_E - \frac{2}{\gamma}\zeta_E^{1/\gamma}$ with $\zeta_E \equiv (\Omega_\Lambda/\Omega_m)^{1/3}$. The details have been explicitly demonstrated in our previous study of RGWs [38,39].

When the NFS is included, a process occurs from a temperature $T \simeq 2$ MeV during the radiation stage up to the beginning of the matter domination; the analytic solution $h_k(\eta)$ has been given [34,38]. The NFS causes a damping of the amplitude of RGWs by ~20% in the frequency range $(10^{-17}, 10^{-10})$ Hz, leaving observable signatures on the second and third peaks of CMB anisotropies and polarization. So the RGWs damped by NFS will be used as a source in our calculation. As for other physical processes, such as the QCD transition and the $e^\pm$ annihilation in the radiation stage [37,40,41], they only cause minor modifications of the RGWs on small scales $\nu > 10^{-12}$ Hz, which are not observable in the present large-scale CMB spectra and will not be considered here.

The solution $h_k(\eta)$ depends on the initial condition during the inflationary stage. We choose the initial spectrum of RGWs at the time η_i of the horizon crossing [34,38,39,42],

$$h(\nu, \eta_i) = \frac{2k^{3/2}}{\pi}|h_k(\eta_i)| = A\left(\frac{k}{k_H}\right)^{2+\beta_{\rm inf}}, \tag{6}$$

where $k_H \simeq 2\pi$ is the comoving wave number corresponding to the Hubble radius, A is a k-independent constant to be normalized by the present observed CMB anisotropies in practice, and the spectral index $\beta_{\rm inf}$ is a parameter depending on inflationary models. The special case of $\beta_{\rm inf} = -2$ is the de Sitter expansion of inflation. If the inflationary expansion is driven by a scalar field, then the index $\beta_{\rm inf}$ is related to the so-called slow-roll parameters, η and ϵ [43], as $\beta_{\rm inf} = -2 + (\eta - 3\epsilon)$. $\beta_{\rm inf}$ is related to the spectral index n_S of primordial scalar perturbations as $n_S = 2\beta_{\rm inf} + 5$. In the literature, the RGW spectrum is also written in the following form [1,2,44]:

$$\Delta_h^2(k) = A_T\left(\frac{k}{k_0}\right)^{n_T} = \frac{1}{8}h^2(\nu, \eta_i), \tag{7}$$

where the tensor spectrum index $n_T = 2(\beta_{\rm inf} + 2) \sim 0$ without the running index, k_0 is some pivot wave number, taken as $k_0 = 0.002\ {\rm Mpc}^{-1}$ in our calculation, and the tensor spectrum amplitude $A_T = 2.95 \times 10^{-9}A(k_0)r$, where $A(k_0)$ is the scalar power spectrum amplitude that can be determined by the WMAP observations [1,3,4], and we take $A(k_0) \sim 0.8$ accordingly. The tensor/scalar ratio r is model dependent, and frequency dependent [33,45]. Recently, the 5-year WMAP data have improved the upper limit to $r < 0.43$ (95% CL) [8], and combined with baryon acoustic oscillation (BAO) and SN this gives $r < 0.2$ (95% CL) [5,7]. In our treatment, for simplicity, $r \simeq 0.37$ is only taken as a constant parameter for normalization of RGWs, unless stated otherwise.

The resulting functions $h_k(\eta)$ and $\dot{h}_k(\eta)$ serve as the tensorial source to CMB anisotropies and polarization. Without reionization, only the RGWs $h_k(\eta_d)$ and $\dot{h}_k(\eta_d)$ at the decoupling time η_d are relevant, contributing to the primary CMB spectra. When reionization begins, $h_k(\eta_r)$ and $\dot{h}_k(\eta_r)$ at the reionization η_r contribute too, mainly to the very large angular reionization bumps of CMB spectra. In Fig. 1, $h_k(\eta_d)$, $\dot{h}_k(\eta_d)$ and $h_k(\eta_r)$, $\dot{h}_k(\eta_r)$ are plotted. The right panel of Fig. 1 shows that $\dot{h}(\eta_d)$ has the greatest amplitude around $k \sim 25$, forming a deep trough, whereas $\dot{h}(\eta_r)$ has the greatest amplitude around $k \sim 2$, forming a deep trough. The left panel shows that both $h_k(\eta_d)$ and $h_k(\eta_r)$ have similar slopes for small k. As we will see, these features of the RGWs at η_d and at η_r are responsible for the profiles of the CMB spectra C_l^{XX}.

III. VISIBILITY FUNCTION

In Basko and Ponarev's method, the Boltzmann equation for the photon gas for the k mode is written as a set of two coupled differential equations [20,21]:

$$\dot{\xi}_k + [ik\mu + q]\xi_k = \dot{h}_k, \tag{8}$$

$$\dot{\beta}_k + [ik\mu + q]\beta_k = qG_k, \tag{9}$$

where β_k is the linear polarization contributed only by linearly polarized CMB photons,

$$\alpha_k \equiv \xi_k - \beta_k \tag{10}$$

is the anisotropy of radiation intensity contributed by both unpolarized (natural light) and polarized CMB photons, $\mu = \cos\theta$, q is the differential optical depth, and

$$G_k(\eta) = \frac{3}{16}\int_{-1}^{1} d\mu'\left[(1+\mu'^2)^2\beta_k - \frac{1}{2}(1-\mu'^2)^2\xi_k\right]. \tag{11}$$

In the following, we omit the subscript k for simplicity of notation. The formal solutions of Eqs. (8) and (9) at any time η can be written as the following time integrations [33,34]:

$$\xi(\eta) = \int_0^{\eta} \dot{h}(\eta')e^{-\kappa(\eta,\eta')}e^{ik\mu(\eta'-\eta)}d\eta', \tag{12}$$

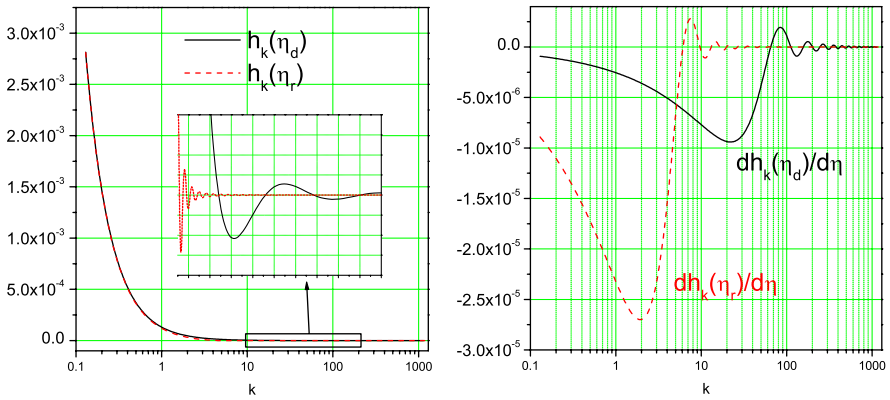

FIG. 1 (color online). The RGWs $h_k(\eta_d)$ and $\dot{h}_k(\eta_d)$ at the decoupling, and $h_k(\eta_r)$ and $\dot{h}_k(\eta_r)$ at the reionization.

$$\beta(\eta) = \int_0^{\mu} G(\eta')q(\eta')e^{-\kappa(\eta,\eta')}e^{ik\mu(\eta'-\eta)}d\eta', \quad (13)$$

where

$$\kappa(\eta', \eta) \equiv \int_{\eta}^{\eta'} q d\eta = \kappa(\eta) - \kappa(\eta') \quad (14)$$

with the optical depth given by

$$\kappa(\eta) \equiv \kappa(\eta_0, \eta) = \int_{\eta}^{\eta_0} q(\eta')d\eta' \quad (15)$$

from the present time η_0 back to an earlier time η, such that

$$q(\eta) = -\frac{d\kappa(\eta)}{d\eta}. \quad (16)$$

The CMB anisotropies and polarization are usually expressed in terms of their Legendre components

$$\xi_l(\eta) = \frac{1}{2}\int_{-1}^{1} d\mu \xi(\eta, \mu)P_l(\mu), \quad (17)$$

$$\beta_l(\eta) = \frac{1}{2}\int_{-1}^{1} d\mu \beta(\eta, \mu)P_l(\mu), \quad (18)$$

where P_l is the Legendre function. By the expansion formula

$$e^{ix\mu} = \sum_{l=0}^{\infty}(2l+1)i^l j_l(x)P_l(\mu) \quad (19)$$

and the orthonormal relation for the Legendre functions, the components at the present time η_0 are given by

$$\xi_l(\eta_0) = i^l \int_0^{\eta_0} e^{-\kappa(\eta)}\dot{h}(\eta)j_l(k(\eta-\eta_0))d\eta, \quad (20)$$

$$\beta_l(\eta_0) = i^l \int_0^{\eta_0} G(\eta)V(\eta)j_l(k(\eta-\eta_0))d\eta, \quad (21)$$

where

$$V(\eta) = q(\eta)e^{-\kappa(\eta)} \quad (22)$$

is the visibility function. As one can see, to analytically carry out the integrations in Eqs. (20) and (21), one needs the explicit expressions of $e^{-\kappa(\eta)}$ and $V(\eta)$, which are determined by the whole history of ionization. In the following, we will give approximate formulas for both functions.

$V(\eta)$ is the probability that a CMB photon reaching us today was last scattered by free electrons at the time η. Without the reionization, $V(\eta)$ would have only one sharp peak around $z \sim 1100$ for the decoupling, and would satisfy the normalization condition

$$\int_0^{\eta_0} V(\eta)d\eta = 1. \quad (23)$$

When the reionization is included, $V(\eta)$ will have, around $z \sim 11$, another peak. If the Universe was reionized twice, say at $z \sim 6$ and $z \sim 16$ [46–48], $V(\eta)$ would have double peaks for reionization. We consider only the case of a single reionization in this paper. Then, as a function of η, $V(\eta)$ is mainly distributed around decoupling and reionization, and is effectively vanishing in the region far away from the peaks, as shown in Fig. 6(d). Thus the time integration of Eq. (23) can be practically split into two parts,

$$\int_0^{\eta_{\rm split}} V_d(\eta)d\eta + \int_{\eta_{\rm split}}^{\eta_0} V_r(\eta)d\eta = 1, \quad (24)$$

where $V_d(\eta)$ and $V_r(\eta)$ are the portions of $V(\eta)$ for decoupling and reionization, respectively, and $\eta_{\rm split}$ is some point between decoupling and reionization with $V(\eta_{\rm split}) \simeq 0$. In the calculation we can take, say, $\eta_{\rm split} = 0.297$ corresponding to a redshift $z \simeq 100$. In Eq. (24), $\int_0^{\eta_{\rm split}} V_d(\eta)d\eta$ is the area covered under the curve of $V_d(\eta)$, and it stands for the probability that a photon was last scattered during the decoupling. Similarly, $\int_{\eta_{\rm split}}^{\eta_0} V_r(\eta)d\eta$ is the probability that a photon was last rescattered during the reionization, i.e., the amount of CMB photons out of the total that are rescattered. According to Eq. (24), their sum is constrained to be unity. This has a physical interpretation: more CMB photons are last scattered around $\sim\eta_r$, and less will be last scattered around $\sim\eta_d$. During reionization the intrinsic anisotropies of this portion of CMB photons were washed out, and new polarizations were generated on large angular scales. As we will see, $\int_{\eta_{\rm split}}^{\eta_0} V_r(\eta)d\eta$ depends essentially on the optical depth up to the reionization.

Now let us specify the visibility functions $V_d(\eta)$ and $V_r(\eta)$. First, we study $V_d(\eta)$ for the decoupling process. It has been given explicitly and it depends on the baryon fraction Ω_B [19,49,50]. As a function of time, the profile of $V_d(\eta)$ itself looks like a sharp peak around the decoupling $z \sim 1100$. Thus, when it appears as a factor of the integrand in the time integration (21) for the polarization $\beta_l(\eta_0)$, it actually plays a filtering role: only the narrow time range around the decoupling contributes substantially to the integral of Eq. (21). To facilitate analytic calculations of CMB polarization, $V_d(\eta)$ has been approximated by the following two pieces of the half-Gaussian function [33,34],

$$V_d(\eta) = \begin{cases} V(\eta_d)\exp(-\frac{(\eta-\eta_d)^2}{2\Delta\eta_{d1}^2}) & (\eta \le \eta_d) \\ V(\eta_d)\exp(-\frac{(\eta-\eta_d)^2}{2\Delta\eta_{d2}^2}) & (\eta > \eta_d), \end{cases} \quad (25)$$

where η_d is the decoupling time, which is taken to be $\eta_d = 0.0707$ corresponding to a redshift $z_d = 1100$, $\Delta\eta_{d1} = 0.006\,39$, $\Delta\eta_{d2} = 0.0117$, and $(\Delta\eta_{d1} + \Delta\eta_{d2})/2 = \Delta\eta_d = 0.009\,05$ is the thickness of the decoupling. Equation (25) improves a single Gaussian function [32] by $\sim$10% in accuracy and at the same time allows an analytic treatment of the CMB polarization spectrum. We have checked that the errors between Eq. (25) and the

numerical formulas given in [19,50] is very small, $\leq 3.9\%$ in the whole range. The coefficient $V(\eta_d)$, as the height of $V_d(\eta)$, also depends on the reionization through the normalization in Eq. (24). The analytic $V_d(\eta)$ with $\Omega_B = 0.046$ and its fitting are shown in Fig. 2.

Next, we study $V_r(\eta)$ for the reionization process. This process is less understood, and various tentative models have been proposed for it. Spatially, the reionization might have occurred inhomogeneously [51–55], resulting in modifications on the small angular scale part of the CMB spectra. Models of double reionization [46,47], or its variants, such as peaklike reionization [56], have also been proposed. In the following, we will work with three simple homogeneous models, whose ionization fraction $X_e(\eta)$ is explicitly given. One is the sudden reionization model with

$$X_e(\eta) = \begin{cases} 0 & \text{for } \eta < \eta_r \\ 1 & \text{for } \eta \geq \eta_r, \end{cases} \tag{26}$$

where η_r is the reionization time. For concreteness of illustration, in our calculation we take $\eta_r = 0.915$, corresponding to the redshift $z_r = 11$. This is the simplest model and is often used in the literature. But there is accumulating evidence that the reionization is an extended process, stretching from $z \simeq 6$ up to $z \sim 11$, even up to as early as $z \sim 20$ [8,57,58]. For instance, studies of Lyα Gunn-Peterson absorption [59] indicate a rapid increase in the ionized fraction of the intergalactic medium at a redshift lower than $z_r \simeq 6$. On the other hand, the WMAP observations of CMB found a much earlier reionization, $z_r = 17 \pm 5$ by WMAP 1-yr [1], $z_r = 10.9^{+2.7}_{-2.3}$ by WMAP 3-yr [3], $z_r = 11.0 \pm 1.4$ (68% CL) by WMAP 5-yr [8], and $z_r = 10.8 \pm 1.4$ by WMAP 5-yr combined with SN and BAO [5,7]. One extended reionization model is the η-linear reionization with

$$X_e(\eta) = \begin{cases} 0 & \text{for } \eta < \eta_{r1} \\ \frac{\eta - \eta_{r1}}{\eta_{r2} - \eta_{r1}} & \text{for } \eta_{r1} < \eta < \eta_{r2} \\ 1 & \text{for } \eta > \eta_{r2}, \end{cases} \tag{27}$$

where η_{r1} and η_{r2} are the beginning and end of reionization. For instance, one can take $\eta_{r1} = 0.685$ and $\eta_{r2} = 1.207\,12$, corresponding to $z_{r1} = 20$ and $z_{r2} = 6$, respectively. This model is closer to the result of WMAP 5-yr fitted by the two-step reionization [8]. Another extended reionization model is the z-linear model with [55]

$$X_e(z) = \begin{cases} 0 & \text{for } z > z_{r1} \\ 1 - \frac{z - z_{r2}}{z_{r1} - z_{r2}} & \text{for } z_{r1} > z > z_{r2} \\ 1 & \text{for } z \leq z_{r2}. \end{cases} \tag{28}$$

For $z_{r1} = 20$ and $z_{r2} = 6$, one has $X_e(z) = 1 - (z - 6)/14$. The ionization fractions $X_e(\eta)$ for these three reionization models are comparatively shown in Fig. 3.

Given $X_e(\eta)$ in the above three models, the differential optical depth for reionization can be directly calculated by the formula [19,55,60]

$$q_r(\eta) = C_c \frac{a(\eta_0)^3}{a(\eta)^2} X_e(\eta), \tag{29}$$

where the constant $C_c = (1 - \frac{Y_p}{2}) \frac{\Omega_b \rho_c \sigma_T}{m_p}$, $Y_p \simeq 0.23$ is the primordial helium fraction, σ_T is the cross section of Thompson scattering, and m_p is the mass of a proton. For $\Omega_b = 0.045$, $C_c \simeq 0.142 \times 10^{-28}$ m^{-1}. Since the value of Y_p from observations has considerably large error bars [61], in our treatment C_c is allowed to vary slightly around this value. From Eq. (15) follows the optical depth for reionization as an integration,

$$\kappa_r(\eta) = \int_{\eta}^{\eta_0} q_r(\eta') d\eta', \tag{30}$$

and, from Eq. (22) follows the visibility function for the reionization,

$$V_r(\eta) = q_r(\eta) e^{-\kappa_r(\eta)}. \tag{31}$$

For instance, for the sudden reionization model, one easily obtains

$$\kappa_r(\eta) = \frac{C_c}{3} \frac{l_H^3}{a_m^2} [(\eta - \eta_m)^{-3} - (\eta_E - \eta_m)^{-3}] + \frac{C_c}{2\gamma + 1} l_H [(\eta_a - \eta_0)^{2\gamma+1} - (\eta_a - \eta_E)^{2\gamma+1}] \quad (\eta \geq \eta_r), \tag{32}$$

where all the parameters have been given below Eq. (5). For a reionization model, the most important quantity $\kappa_r \equiv \kappa_r(\eta_b)$ is the value of the optical depth from η_0 back up to some time η_b before the reionization, where $q_r(\eta_b)$ is practically vanishing. For example, one can take $\eta_b = \eta_{\rm split}$. In practice, one can conveniently take $\eta_b = \eta_r$ for the sudden model, and take $\eta_b = 0.5$ for the η-linear and z-linear models. κ_r is an integral constraint on the reionization history. On the observational side, based upon treatments of a sudden model, WMAP 1-yr gives $\kappa_r = 0.17 \pm 0.04$ [1], WMAP 3-yr gives $\kappa_r = 0.09 \pm 0.03$ [3], WMAP 5-yr gives $\kappa_r = 0.087 \pm 0.017$ [8], and WMAP 5-yr combined with SN and BAO yields

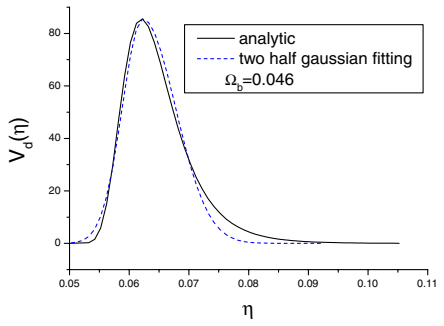

FIG. 2 (color online). The visibility function $V_d(\eta)$ for the decoupling around $z \sim 1100$. Both the analytic fitting and the fitting by two half-Gaussian functions are shown.

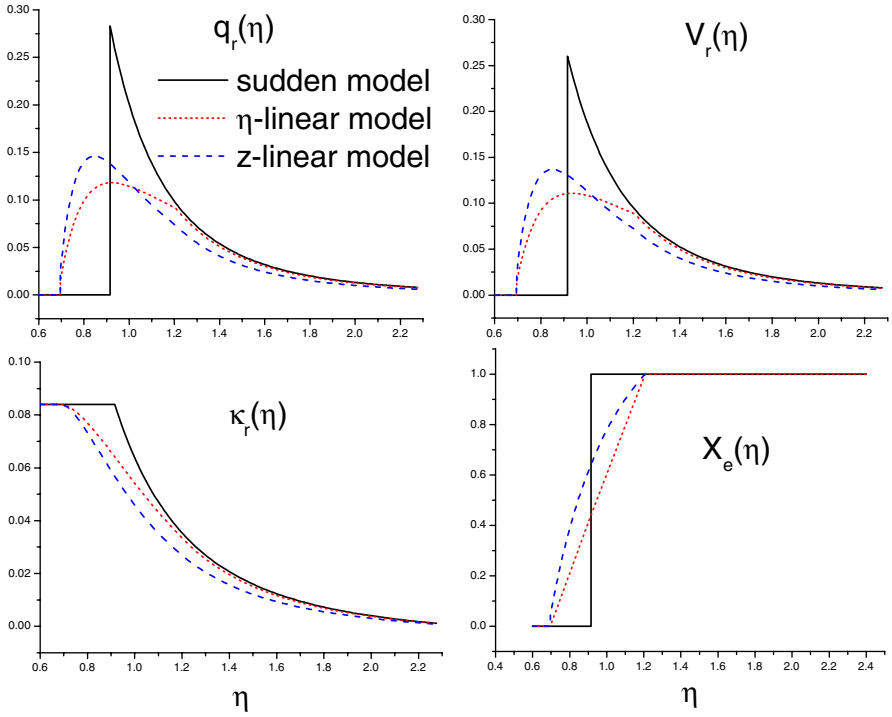

FIG. 3 (color online). The three models of reionization with a fixed optical depth $\kappa_r = 0.084$. For each $X_e(\eta)$ given in Eqs. (26)–(28), the functions $q_r(\eta)$, $\kappa_r(\eta)$, and $V_r(\eta)$ are calculated according to Eqs. (29)–(31), respectively.

$\kappa_r = 0.084 \pm 0.016$ [5,7]. To be specific in our calculation, we will take the value $\kappa_r = 0.084$ for all three reionization models in this paper, except when stated otherwise. However, note that, for extended reionization models, one should be careful in applying the WMAP observed value of κ_r, as it is obtained by using a sudden model. For the η-linear model with $X_e(\eta)$ given in Eq. (27), one uses Eqs. (29)–(31) to compute $q_r(\eta)$, $\kappa_r(\eta)$, $V_r(\eta)$. For the z-linear model with $X_e(\eta)$ in Eq. (28), one does similar computations. The resulting $q_r(\eta)$, $\kappa_r(\eta)$, and $V_r(\eta)$ for these three models are plotted in Fig. 3.

The value of the optical depth κ_r determines the area $\int_{\eta_{\rm split}}^{\eta_0} V_r(\eta)d\eta$ introduced in Eq. (24). For a fixed $\kappa_r = 0.084$, the integration of Eq. (31) yields $\int_{\eta_{\rm split}}^{\eta_0} V_r(\eta)d\eta = 0.0795$ in the sudden model, $\int_{\eta_{\rm split}}^{\eta_0} V_r(\eta)d\eta = 0.07953$ in the η-linear model, and $\int_{\eta_{\rm split}}^{\eta_0} V_r(\eta)d\eta = 0.07973$ in the z-linear model, respectively. So, two gradual models have slightly larger area than the sudden model. Besides, our computations also show that a larger κ_r yields a larger $\int_{\eta_{\rm split}}^{\eta_0} V_r(\eta)d\eta$ and a smaller $\int_0^{\eta_{\rm split}} V_d(\eta)d\eta$ due to Eq. (24); i.e., a larger κ_r increases the possibility that a CMB photon reaching us was last scattered at reionization. As we shall see explicitly, for CMB spectra, this will enhance the reionization bumps on large scales and reduce the primary peaks due to decoupling.

To facilitate analytical calculations of CMB polarization, similar to the treatments of $V_d(\eta)$ for the decoupling, $V_r(\eta)$ can also be approximated by some fitting formula. For the η-linear model, it is fitted by the following two pieces of half-Gaussian functions:

$$V_r(\eta) = \begin{cases} V(\eta_r)\exp(-\frac{(\eta-\eta_r)^2}{2(\Delta\eta_{r1})^2}) & (\eta < \eta_r) \\ V(\eta_r)\exp(-\frac{(\eta-\eta_r)^2}{2(\Delta\eta_{r2})^2}) & (\eta > \eta_r), \end{cases} \tag{33}$$

where $\Delta\eta_{r1} = 0.147$, $\Delta\eta_{r2} = 0.425$, $\Delta\eta_r = (\Delta\eta_{r1} + \Delta\eta_{r2})/2 = 0.286$, and $\eta_r = 0.935$ ($z_r = 10.5$). It is plotted in Fig. 4(c) under the requirement that it gives the same area $\int_{\eta_{\rm split}}^{\eta_0} V_r(\eta)d\eta$ as the one calculated. For the z-linear model, the fitting formula is similar to Eq. (33) but with the parameters $\Delta\eta_{r1} = 0.100$, $\Delta\eta_{r2} = 0.366$, $\Delta\eta_r = (\Delta\eta_{r1} + \Delta\eta_{r2})/2 = 0.233$, and $\eta_r = 0.855$ ($z_r = 13$). It is plotted in Fig. 5(c). Here, for the two extended models, the value of η_r has been taken to correspond to the maximum of $V_r(\eta)$. For the sudden model, it can be fitted by half a piece of the Gaussian function,

$$V_r(\eta) = \begin{cases} 0 & (\text{for } \eta < \eta_r) \\ V(\eta_r)\exp(-\frac{(\eta-\eta_r)^2}{2(\Delta\eta_{dr})^2}) & (\text{for } \eta > \eta_r), \end{cases} \tag{34}$$

with the width $\Delta\eta_{dr} = 0.247$, as plotted in Fig. 6(c). The half-Gaussian fitting of $V_r(\eta)$ for the sudden model is not as accurate as those for the two extended models. It should be expected that in the sudden model the analytical CMB spectra C_l^{XX} based on the fitting formula (34) are not as good as those in the two extended models.

We mention that, given a fixed κ_r, the respective heights $V(\eta_r)$ in Eqs. (26), (33), and (34) are also determined

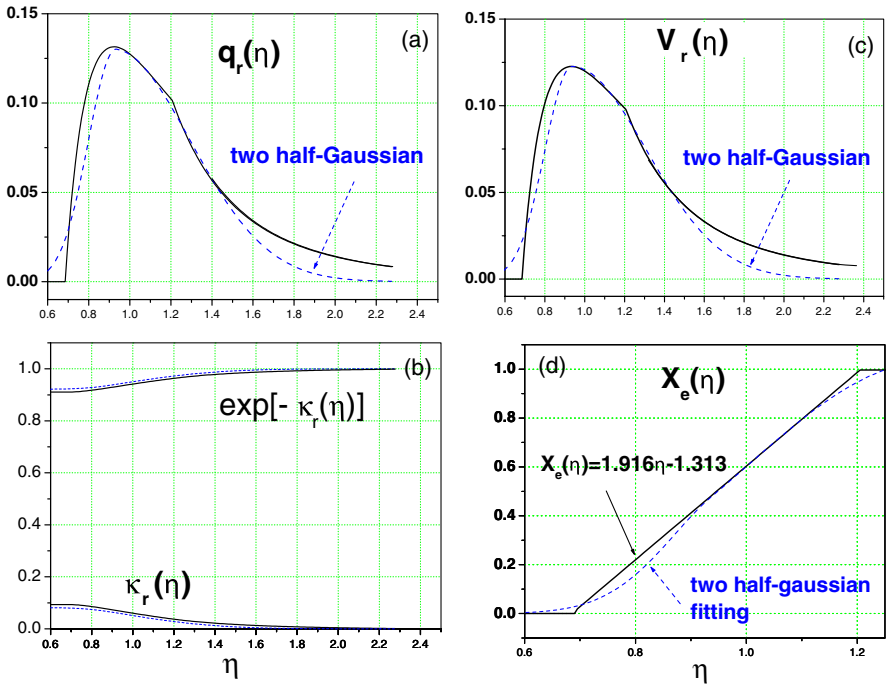

FIG. 4 (color online). The η-linear reionization model with $\kappa_r = 0.084$. The solid lines are the calculated results. The dashed lines are the fittings by two half-Gaussian functions in Eq. (33).

automatically. From these fittings $V_r(\eta)$, one can convert it to obtain the corresponding optical functions,

$$e^{-\kappa_r(\eta)} = 1 - \int_{\eta}^{\eta_0} V_r(\eta) d\eta, \tag{35}$$

$$\kappa_r(\eta) = -\ln\left(1 - \int_{\eta}^{\eta_0} V_r(\eta) d\eta\right), \tag{36}$$

$$q_r(\eta) = \frac{V_r(\eta)}{(1 - \int_{\eta}^{\eta_0} V_r(\eta) d\eta)}. \tag{37}$$

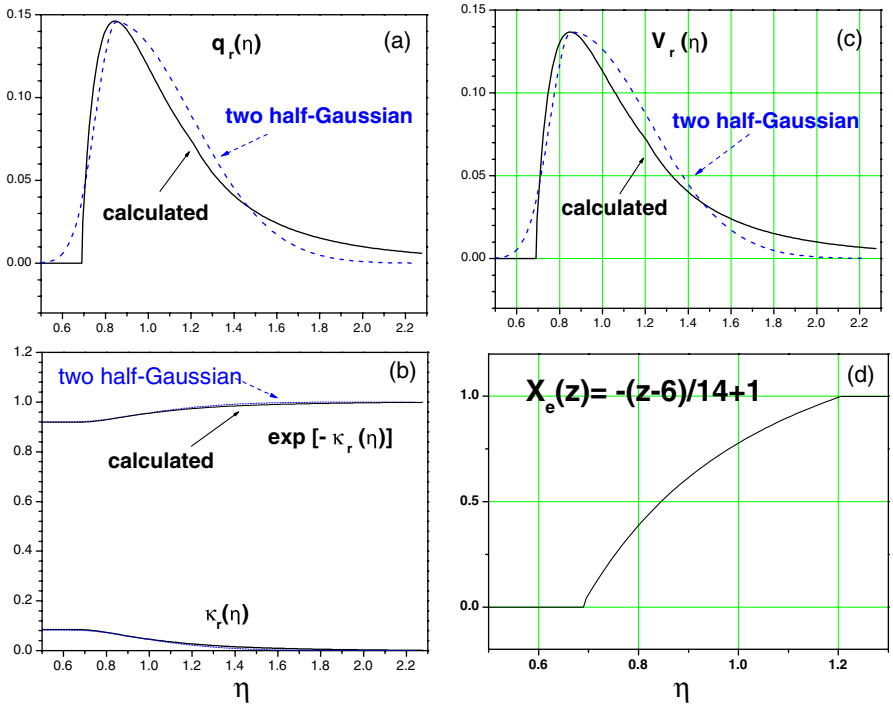

FIG. 5 (color online). The z-linear reionization model and its fitting.

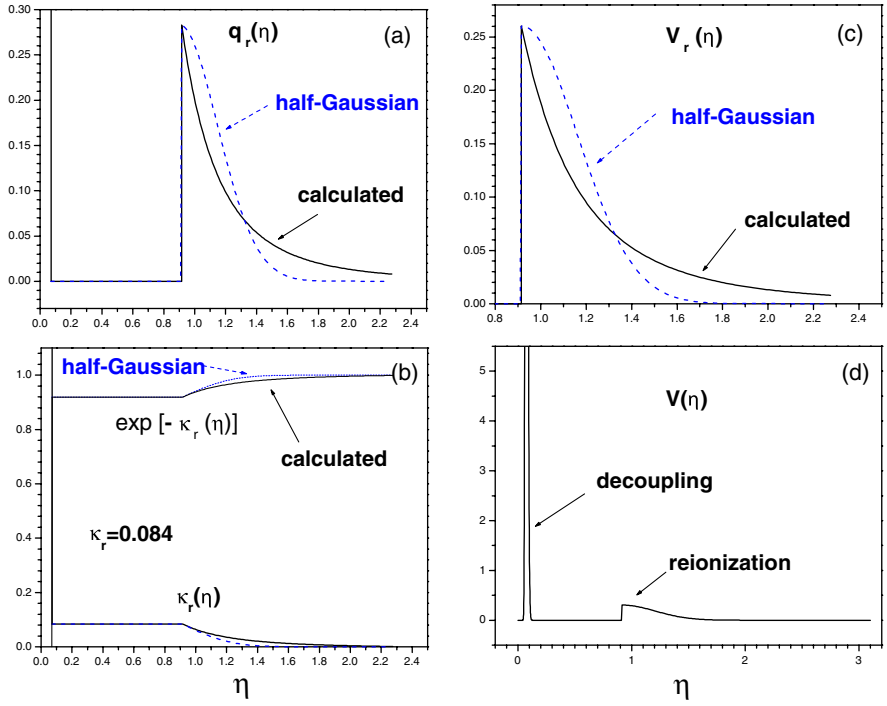

FIG. 6 (color online). The sudden reionization model and its fitting. Panel (c) shows that the fitting $V_r(\eta)$ from Eq. (34) has large errors compared to the calculated one. The evolution history of $V(\eta)$, including both reionization and decoupling, is sketched in panel (d).

It should be mentioned that the approximate fitting of $V_r(\eta)$ by Eq. (33) underestimates the value of V_r in the range $\eta > \eta_r$ by $\sim 9.1\%$. For the z-linear model, the fitting by half-Gaussian functions underestimates the value of V_r in the range $\eta > \eta_r$ by $\sim 8.6\%$. However, this kind of error of the fitting can be partially compensated in treating the damping factors occurring in the time integration of the polarization mode, as will be given in the following. The Gaussian fitting of Eq. (34) for the sudden model is included only for illustration purposes, as its error is larger than in the two extended models.

IV. SPECTRA OF CMB ANISOTROPIES AND POLARIZATION

By applying the same kind of approximate integration technique as in Refs. [33,34], up to the second order of a small $1/q^2$ in the tight coupling limit, the function $G(\eta)$ in Eq. (11) can be written as

$$G(\eta) = -\frac{1}{10}\int_0^{\eta} \dot{h}(\eta')e^{-(3/10)\kappa(\eta')-(7/10)\kappa(\eta)}d\eta', \quad (38)$$

and the integration of the polarization mode in Eq. (21) is written as

$$\beta_l(\eta_0) = -\frac{1}{10}i^l\int_0^{\eta_0} d\eta V(\eta)\dot{h}(\eta)j_l(k(\eta-\eta_0)) \times \int_0^{\eta} d\eta' e^{-(3/10)\kappa(\eta')-(7/10)\kappa(\eta)}. \quad (39)$$

Since the visibility function $V(\eta)$ for the whole history consists of two effectively nonoverlapping functions, $V_d(\eta)$ and $V_r(\eta)$, the η time integration $\int_0^{\eta_0} d\eta$ in the above is naturally split into a sum of two integrations:

$$\begin{aligned}\beta_l(\eta_0) = &-\frac{1}{10}i^l\int_0^{\eta_{\rm split}} d\eta V_d(\eta)\dot{h}(\eta)j_l(k(\eta-\eta_0)) \\ &\times \int_0^{\eta} d\eta' e^{-(3/10)\kappa(\eta')-(7/10)\kappa(\eta)} \\ &-\frac{1}{10}i^l\int_{\eta_{\rm split}}^{\eta_0} d\eta V_r(\eta)\dot{h}(\eta)j_l(k(\eta-\eta_0)) \\ &\times \int_0^{\eta} d\eta' e^{-(3/10)\kappa(\eta')-(7/10)\kappa(\eta)}. \end{aligned} \quad (40)$$

One defines the integration variable $x \equiv \kappa(\eta')/\kappa(\eta)$ to replace the variable η' in the above equation. Since $V_d(\eta)$ is peaked around η_d with a width $\Delta\eta_d$, and, similarly, $V_r(\eta)$ is peaked around η_r with a width $\Delta\eta_r$, one can take $d\eta' \simeq -\Delta\eta_d\frac{dx}{x}$ and $d\eta' \simeq -\Delta\eta_r\frac{dx}{x}$ as approximations, respectively,

$$\begin{aligned}\beta_l(\eta_0) = &-\frac{1}{10}i^l\Delta\eta_d\int_0^{\eta_{\rm split}} d\eta V_d(\eta)\dot{h}(\eta)j_l(k(\eta-\eta_0)) \\ &\times \int_1^{\infty}\frac{dx}{x}e^{-(3/10)\kappa(\eta)x-(7/10)\kappa(\eta)} \\ &-\frac{1}{10}i^l\Delta\eta_r\int_{\eta_{\rm split}}^{\eta_0} d\eta V_r(\eta)\dot{h}(\eta)j_l(k(\eta-\eta_0)) \\ &\times \int_1^{\infty}\frac{dx}{x}e^{-(3/10)\kappa(\eta)x-(7/10)\kappa(\eta)}. \end{aligned} \quad (41)$$

For each term in the above equation, the η time integration can be dealt with, using the same kind of treatment as in Refs. [33,34]. For the decoupling one has

$$\int_0^{\eta_{\rm split}} d\eta V_d(\eta)\dot{h}(\eta) j_l(k(\eta-\eta_0)) \simeq D_d(k)\dot{h}(\eta_d) j_l(k(\eta_d-\eta_0)) \int_0^{\eta_{\rm split}} d\eta V_d(\eta), \quad (42)$$

where the damping factor for the decoupling is given by the following fitting formula,

$$D_d(k) = \frac{1.4}{2}[e^{-c(k\Delta\eta_{d1})^b} + e^{-c(k\Delta\eta_{d2})^b}], \quad (43)$$

which can be simplified by

$$D_d(k) = 1.4 e^{-c(k\Delta\eta_d)^b}, \quad (44)$$

with c and b being two fitting parameters. For CMB spectra without reionization, it has been shown in Ref. [34] that both damping factors in Eqs. (43) and (44), $c \simeq 0.6$ and $b \simeq 0.85$, are a good match for the numerical result given by CAMB [16] over an extended range $l \leq 600$, covering the first three primary peaks, and the error is only $\sim 3\%$.

Similarly, the η time integration for the reionization is

$$\int_{\eta_{\rm split}}^{\eta_0} d\eta V_r(\eta)\dot{h}(\eta) j_l(k(\eta-\eta_0)) \simeq D_r(k)\dot{h}(\eta_r) j_l(k(\eta_r-\eta_0)) \int_{\eta_{\rm split}}^{\eta_0} d\eta V_d(\eta), \quad (45)$$

where the damping factor for the extended models is taken to be

$$D_r(k) = \frac{1.4}{2}[e^{-c(k\Delta\eta_{r1})^b} + e^{-c(k\Delta\eta_{r2})^b}], \quad (46)$$

or for the sudden reionization,

$$D_r(k) = \frac{1.4}{2} e^{-c(k\Delta\eta_r)^b}. \quad (47)$$

Here the parameters c and b in Eqs. (46) and (47) for reionization could take values different from those for decoupling. For simplicity, we let them take the values that are the same as in $D_d(k)$. Guided by the error estimation for the decoupling case, we can only estimate the errors due to $D_r(k)$ in Eq. (46) for the two extended models, upon the reionization bumps of polarization spectra, to be $\leq 10\%$, the same order of magnitude as those of the fitting $V_r(\eta)$ in Eq. (33).

Substituting Eqs. (42) and (45) into Eq. (41), and performing the integrations $\int d\eta$ first,

$$\int_0^{\eta_{\rm split}} d\eta V_d(\eta) e^{-(3/10)\kappa(\eta)x-(7/10)\kappa(\eta)} = \int_{\kappa_r}^{\infty} d\kappa e^{-(3/10)\kappa x-(17/10)\kappa} = \frac{1}{\frac{17}{10}+\frac{3}{10}x} e^{-((17/10)+(3/10)x)\kappa_r}, \quad (48)$$

$$\int_{\eta_{\rm split}}^{\eta_0} d\eta V_r(\eta) e^{-(3/10)\kappa(\eta)x-(7/10)\kappa(\eta)} = \int_0^{\kappa_r} d\kappa e^{-(3/10)\kappa x-(17/10)\kappa} = \frac{1}{\frac{17}{10}+\frac{3}{10}x}[1 - e^{-((17/10)+(3/10)x)\kappa_r}], \quad (49)$$

one finally obtains the expression of the polarization mode as a sum of two parts,

$$\beta_l(\eta_0) = -\frac{1}{10} i^l [A_1(\kappa_r) D_d(k) \Delta\eta_d \dot{h}(\eta_d) j_l(k(\eta_d-\eta_0)) + A_2(\kappa_r) D_r(k) \Delta\eta_r \dot{h}(\eta_r) j_l(k(\eta_r-\eta_0))] \quad (50)$$

where the κ_r-dependent coefficients

$$A_1(\kappa_r) = \int_1^{\infty} \frac{dx}{x(\frac{17}{10}+\frac{3}{10}x)} e^{-((17/10)+(3/10)x)\kappa_r}, \quad (51)$$

$$A_2(\kappa_r) = \int_1^{\infty} \frac{dx}{x(\frac{17}{10}+\frac{3}{10}x)}[1 - e^{-((17/10)+(3/10)x)\kappa_r}], \quad (52)$$

both being independent of the wave number k, and the sum is $A_1(\kappa_r) + A_2(\kappa_r) = \frac{10}{17}\ln\frac{20}{3} \simeq 1.116$, which is independent of κ_r. If one sets $A_2 = 0$ and $A_1 = \frac{10}{17}\ln\frac{20}{3}$, Eq. (50) reduces to exactly that of the nonreionization case [33,34]. Actually, after the sum is normalized to unity, the two coefficients have the physical meaning that

$$a_1(\kappa_r) \equiv \frac{A_1(\kappa_r)}{\frac{10}{17}\ln\frac{20}{3}} \quad (53)$$

is the probability that a polarized photon we perceive was last scattered during the decoupling epoch, and

$$a_2(\kappa_r) \equiv \frac{A_2(\kappa_r)}{\frac{10}{17}\ln\frac{20}{3}} \quad (54)$$

is the probability that a polarized photon we perceive was last scattered during the time interval from the beginning of reionization up to the present time η_0. It is found that $a_1(\kappa_r)$ is a decreasing function of κ_r and $a_2(\kappa_r)$ is an increasing one, as shown in Fig. 7. Therefore, if more CMB photons are scattered by the free electrons during the reionization, the optical depth κ_r acquires a larger value, giving rise to a higher coefficient $A_2(\kappa_r)$ and, at the same time, a lower coefficient $A_1(\kappa_r)$. The $A_1(\kappa_r)$ part in β_l from the decoupling will give rise to the primary peaks of C_l^{EE} and C_l^{BB}, and will be prominent on small

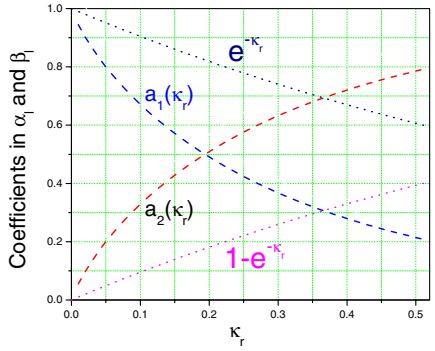

FIG. 7 (color online). The normalized coefficients $a_1(\kappa_r)$ and $a_2(\kappa_r)$ of the polarization β_l. A larger κ_r yields lower $a_1(\kappa_r)$ and higher $a_2(\kappa_r)$, i.e., lower primary peaks and higher reionization bumps in C_l^{EE} and C_l^{BB}. Also plotted are the coefficients $e^{-\kappa_r}$ and $(1-e^{-\kappa_r})$ of the temperature anisotropies α_l. Notice that $a_1(\kappa_r)$ and $a_2(\kappa_r)$ vary with κ_r more drastically than $e^{-\kappa_r}$ and $(1-e^{-\kappa_r})$, respectively.

angular scales with $l \geq 100$. The $A_2(\kappa_r)$ part from the reionization will be dominant on large angular scales and will yield the reionization bumps of C_l^{EE} and C_l^{BB} around $l < 10$.

The analytical expression (50) shows that effects of relevant physical elements upon the polarization have been explicitly isolated and displayed. The κ_r dependence of β_l is attributed to the coefficients $A_1(\kappa_r)$ and $A_2(\kappa_r)$, which determine the relative heights of the primary peaks and the reionization bump. Other effects of reionization are encoded in the factor $D_r(k)\Delta\eta_r$. The effects of decoupling are absorbed in $D_d(k)\Delta\eta_d$. The effects of RGWs upon the polarization are given by the time derivatives $\dot{h}(\eta_d)$ at η_d and $\dot{h}(\eta_r)$ at η_r, which not only contain the cosmological information of inflation, NFS, etc., but also determine the overall profiles of C_l^{EE} and C_l^{BB}, such as the locations of peaks and troughs, and of bumps. The factors $j_l(k(\eta_d - \eta_0))$ and $j_l(k(\eta_r - \eta_0))$ just play the role of conversion from the wave number k space into the multipole l space.

To calculate the temperature anisotropies, we need to evaluate ξ_l in Eq. (20), which contains the factor $e^{-\kappa(\eta)}$. This also needs to be dealt with properly. As shown in Fig. 6, the factor $e^{-\kappa(\eta)}$ has two steps, one at the decoupling $\eta = \eta_d$ and another at $\eta \simeq \eta_r$ caused by the reionization. It can be approximated by the following two-step function:

$$e^{-\kappa(\eta)} \simeq \begin{cases} 0 & (\eta < \eta_d) \\ e^{-\kappa_r} & (\eta_d < \eta < \eta_r) \\ 1 & (\eta_r < \eta < \eta_0), \end{cases} \tag{55}$$

and its reionization-relevant part $e^{-\kappa_r(\eta)}$ is between (η_d, η_0). From Eq. (35), $e^{-\kappa_r(\eta)}$ is the integration of $V_r(\eta)$ from η to η_0, determined by the area under the curve of $V_r(\eta)$, and is not very sensitive to the detailed shape of $V_r(\eta)$. Therefore, the approximate formula (55) will be used for the three models of reionization, with their respective values of η_r. Note that Eq. (55) tends to overestimate the contribution of the reionization to the integration, since $e^{-\kappa(\eta)}$, shown in Fig. 6, increases gradually from $e^{-\kappa_r}$ at η_r up to 1 for $\eta \gg \eta_r$, instead of instantaneously jumping up to 1 at η_r. To compensate for this overestimation, in actually calculating $\xi_l(\eta_0)$ in the linear model, we may use the value of η_r slightly greater than 0.935. But this adjustment of the time η_r does not apply to $\beta_l(\eta_0)$ in Eq. (50). Substituting Eq. (55) into Eq. (20), the integration for ξ_l is split into two terms:

$$\xi_l(\eta_0) \simeq i^l \int_{\eta_d}^{\eta_r} e^{-\kappa_r} \dot{h}(\eta) j_l(k(\eta_0 - \eta)) d\eta + i^l \int_{\eta_r}^{\eta_0} \dot{h}(\eta) j_l(k(\eta_0 - \eta)) d\eta. \tag{56}$$

Following the similar treatments in [34,45], each term is integrated by parts, yielding the following approximate expression:

$$\xi_l(\eta_0) = -i^l [e^{-\kappa_r} h(\eta_d) j_l(k(\eta_0 - \eta_d)) + (1 - e^{-\kappa_r}) h(\eta_r) j_l(k(\eta_0 - \eta_r))], \tag{57}$$

where the first term is generated by $h(\eta_d)$ at the recombination and the second term is due to $h(\eta_r)$ at the reionization. Equation (10) then yields the mode of CMB temperature anisotropies $\alpha_l(\eta_0) = \xi_l(\eta_0) - \beta_l(\eta_0)$. In fact, $\alpha_l(\eta_0)$ is essentially contributed by $\xi_l(\eta_0)$ since the amplitude of $\xi_l(\eta_0)$ is about 2 orders higher than that of $\beta_l(\eta_0)$. Written explicitly, one has the approximate, analytic expression of the mode of CMB temperature anisotropies, including the reionization,

$$\alpha_l(\eta_0) = -i^l j_l(k(\eta_0 - \eta_d)) \left[e^{-\kappa_r} h(\eta_d) - \frac{1}{10} A_1(\kappa_r) D_d(k) \Delta\eta_d \dot{h}(\eta_d) \right] - i^l j_l(k(\eta_0 - \eta_r)) \left[(1 - e^{-\kappa_r}) h(\eta_r) - \frac{1}{10} A_2(\kappa_r) D_r(k) \Delta\eta_{dr} \dot{h}(\eta_r) \right]. \tag{58}$$

In this expression, the first term containing $h(\eta_d)$ and $\dot{h}(\eta_d)$ is brought in by the decoupling and is responsible for the primary peaks, whereas the last term containing $h(\eta_r)$ and $\dot{h}(\eta_r)$ is brought in by reionization and is prominent on large angular scales with $l < 10$. When one sets $A_1 = 1$, $A_2 = 0$, and $e^{-\kappa_r} = 1$, Eq. (58) reduces to the results for the case without reionization [34]. The κ_r dependence of α_l is mainly attributed to the factors $e^{-\kappa_r}$ and $(1 - e^{-\kappa_r})$, while the portion containing $A_1(\kappa_r)$ and $A_2(\kappa_r)$ is the subdominant β_l. From Eq. (35) and the definition of κ_r, one has

$$e^{-\kappa_r} = 1 - \int_{\eta_b}^{\eta_0} V_r(\eta) d\eta, \tag{59}$$

which has a physical interpretation: the probability of a CMB photon being last scattered during the earlier epoch before the reionization. Since $e^{-\kappa_r} < 1$ for $\kappa_r > 0$, this will cause a slight decrease in the amplitude of the temperature anisotropies, as demonstrated in Eq. (58). Correspondingly, the factor $(1 - e^{-\kappa_r})$ in front of $h(\eta_r)$ is

$$1 - e^{-\kappa_r} = \int_{\eta_b}^{\eta_0} V_r(\eta) d\eta, \tag{60}$$

which is recognized as the probability of a CMB photon being last scattered during the time interval from the reionization up to the present time η_0. These foregoing probabilistic interpretations are parallel to the case of CMB anisotropies generated by scalar perturbations, where reionization also brings about a similar exponential factor $e^{-\kappa_r}$ in the temperature anisotropies, and a physical illustration of its appearance is given in Ref. [62]. It should be mentioned that the probabilities in Eqs. (59) and (60) are, respectively, different from the normalized $a_1(\kappa_r)$ and $a_2(\kappa_r)$; the latter are for the polarized photons. Moreover, as shown in Fig. 7, $a_1(\kappa_r)$ decreases with κ_r much faster than $e^{-\kappa_r}$ does, and $a_2(\kappa_r)$ increases much faster than $(1 - e^{-\kappa_r})$. In this sense, the polarization $\beta_l(\eta_0)$ is more sensitive to κ_r than the temperature anisotropies $\alpha_l(\eta_0)$. Therefore, one may say that the polarization spectra C_l^{EE} and C_l^{BB} are more sensitive probes into the reionization than the temperature anisotropy spectrum C_l^{TT}.

When α_l and β_l are ready, one can compute straightforwardly the CMB spectra caused by RGWs. The detailed derivations have been demonstrated in Refs. [25,33,34]. In particular, some minor misprints of the coefficients in Ref. [25] have been pointed out and corrected in Refs. [33,34]. The spectrum of temperature anisotropies is

$$C_l^{TT} = \frac{1}{8\pi}\frac{(l+2)!}{(l-2)!}\int k^2 dk \left| \frac{\alpha_{l-2}(\eta_0)}{(2l-1)(2l+1)} - \frac{2\alpha_l(\eta_0)}{(2l-1)(2l+3)} + \frac{\alpha_{l+2}(\eta_0)}{(2l+1)(2l+3)} \right|^2, \tag{61}$$

the spectrum of the electric type of polarization is

$$C_l^{EE} = \frac{1}{16\pi}\int k^2 dk \left| \frac{(l+1)(l+2)\beta_{l-2}(\eta_0)}{(2l-1)(2l+1)} + \frac{6(l-1)(l+2)\beta_l(\eta_0)}{(2l-1)(2l+3)} + \frac{l(l-1)\beta_{l+2}(\eta_0)}{(2l+1)(2l+3)} \right|^2, \tag{62}$$

the spectrum of the magnetic type of polarization is

$$C_l^{BB} = \frac{1}{16\pi}\int k^2 dk \left| \frac{2(l+2)\beta_{l-1}(\eta_0)}{(2l+1)} + \frac{2(l-1)\beta_{l+1}(\eta_0)}{(2l+1)} \right|^2, \tag{63}$$

and the cross spectrum of temperature polarization is

$$C_l^{TE} = \sqrt{\frac{1}{8\pi}\frac{(l+2)!}{(l-2)!}}\sqrt{\frac{1}{16\pi}}\int k^2 dk \left[\frac{\alpha_{l-2}(\eta_0)}{(2l-1)(2l+1)} - \frac{2\alpha_l(\eta_0)}{(2l-1)(2l+3)} + \frac{\alpha_{l+2}(\eta_0)}{(2l+1)(2l+3)} \right] \times \left[\frac{(l+1)(l+2)\beta_{l-2}(\eta_0)}{(2l-1)(2l+1)} + \frac{6(l-1)(l+2)\beta_l(\eta_0)}{(2l-1)(2l+3)} + \frac{l(l-1)\beta_{l+2}(\eta_0)}{(2l+1)(2l+3)} \right]. \tag{64}$$

Substituting $\alpha_l(\eta_0)$ and $\beta_l(\eta_0)$ into Eqs. (61)–(64) yields the analytical expressions of the spectra of CMB with the modifications of reionization:

$$C_l^{TT} = \frac{1}{8\pi}\frac{(l+2)!}{(l-2)!}\int k^2 dk \left\{ P_{Tl}(k(\eta_0 - \eta_d)) \left[e^{-\kappa_r} h(\eta_d) - \frac{1}{10} A_1 D_d(k) \Delta\eta_d \dot{h}(\eta_d) \right] + P_{Tl}(k(\eta_0 - \eta_r)) \times \left[(1 - e^{-\kappa_r}) h(\eta_r) - \frac{1}{10} A_2 D_r(k) \Delta\eta_r \dot{h}(\eta_r) \right] \right\}^2, \tag{65}$$

$$C_l^{EE} = \frac{1}{16\pi}\left(\frac{1}{10}\right)^2 \int k^2 dk [P_{El}(k(\eta_0 - \eta_d)) \times A_1 D_d(k) \Delta\eta_d \dot{h}(\eta_d) + P_{El}(k(\eta_0 - \eta_r)) \times A_2 D_r(k) \Delta\eta_r \dot{h}(\eta_r)]^2, \tag{66}$$

$$C_l^{BB} = \frac{1}{16\pi}\left(\frac{1}{10}\right)^2 \int k^2 dk [P_{Bl}(k(\eta_0 - \eta_d)) \times A_1 D_d(k) \Delta\eta_d \dot{h}(\eta_d) + P_{Bl}(k(\eta_0 - \eta_r)) \times A_2 D_r(k) \Delta\eta_r \dot{h}(\eta_r)]^2, \tag{67}$$

$$C_l^{TE} = -\frac{1}{8\sqrt{2}\pi \times 10}\sqrt{\frac{(l+2)!}{(l-2)!}}\int k^2 dk \frac{1}{2}\left\{ \left[P_{Tl}(k(\eta_0 - \eta_d)) \left[e^{-\kappa_r} h(\eta_d) - \frac{1}{10} A_1 D_d(k) \Delta\eta_d \dot{h}(\eta_d) \right] + P_{Tl}(k(\eta_0 - \eta_r)) \left[(1 - e^{-\kappa_r}) h(\eta_r) - \frac{1}{10} A_2 D_r(k) \Delta\eta_{dr} \dot{h}(\eta_r) \right] \right] \left[P_{El}(k(\eta_0 - \eta_d)) A_1 D_d(k) \Delta\eta_d \dot{h}(\eta_d) + P_{El}(k(\eta_0 - \eta_r)) A_2 D_r(k) \Delta\eta_r \dot{h}(\eta_r) \right]^* + \text{complex conjugate} \right\}. \tag{68}$$

In the above integrations, the projection factors are defined as

$$P_{Tl}(x) = \frac{j_{l-2}(x)}{(2l-1)(2l+1)} + \frac{2j_l(x)}{(2l-1)(2l+3)} + \frac{j_{l+2}(x)}{(2l+1)(2l+3)} = \frac{j_l(x)}{x^2}, \quad (69)$$

$$P_{El}(x) = \frac{(l+1)(l+2)}{(2l-1)(2l+1)} j_{l-2}(x) - \frac{6(l-1)(l+2)}{(2l-1)(2l+3)} j_l(x) + \frac{l(l-1)}{(2l+1)(2l+3)} j_{l+2}(x) = -\left[2 - \frac{l(l-1)}{x^2}\right] j_l(x) + \frac{2}{x} j_{l-1}(x), \quad (70)$$

$$P_{Bl}(x) = \frac{2(l+2)}{(2l+1)} j_{l-1}(x) - \frac{2(l-1)}{(2l+1)} j_{l+1}(x) = 2j_{l-1}(x) - 2\frac{l-1}{x} j_l(x). \quad (71)$$

We apply these formulas to the three reionization models, respectively, and plot the spectra C_l^{XX}. The reionized spectra C_l^{XX} are plotted in Fig. 8 for the three models of reionization, in which we also plot the numerical spectra from the CAMB online tool for a comparison [16]. Both the analytic and numerical computations use the same set of parameters, $\kappa_r = 0.084$ and $r = 0.37$. On large scales $l \leq 600$, our analytical C_l^{EE} and C_l^{BB} agree with the numerical ones. For the two extended models, the error is $\sim 3\%$ for the primary peaks, and the error is estimated to be $\leq 15\%$ for the reionization bumps, which is superposed by that of decoupling $\sim 3\%$ and that of reionization $\sim 10\%$. Notice also that the analytical C_l^{EE} and C_l^{BB} in the sudden model have reionization bumps that are too low. This is expected, since the half-Gaussian fitting formula (34) is poor. The analytical C_l^{TT} and C_l^{TE} are close to the numerical ones on smaller scales, $l > 20$, but have an obvious departure from the numerical ones on very large scales, $l < 10$. This implies that the approximation of temperature anisotropies ξ_l in Eq. (57) is poor for small multipoles, $l < 10$. In the following we focus only on the two extended models and examine the impact of reionization through the analytical spectra C_l^{XX}.

V. EFFECTS OF REIONIZATION

1. The most prominent modification due to the reionization is that it enhances the low-l parts of the spectra, forming a reionization bump at $l \sim 5$ for C_l^{EE} and C_l^{BB}, respectively. The position of this bump is a reflection of the horizon scale at reionization, whose corresponding angular scale, $l \sim 5$, is much larger than $l \sim 100$ of the primary peaks at the photon decoupling. As pointed out earlier, the profiles of C_l^{XX} are determined by the profiles of RGWs at the decoupling and at the reionization as well. In particular, the reionization bumps are generated by $\dot{h}(\eta_r)$, and the primary peaks and troughs are due to $h(\eta_d)$ and $\dot{h}(\eta_d)$. This correspondence is clearly demonstrated by Fig. 9, in which the left panel plots C^{EE} and C^{BB}, as well as $\dot{h}(\eta_d)$ and $\dot{h}(\eta_r)$ in one graph, and the right panel plots C^{TT}, as well as $h(\eta_d)$ and $h(\eta_r)$ in one graph. This correspondence

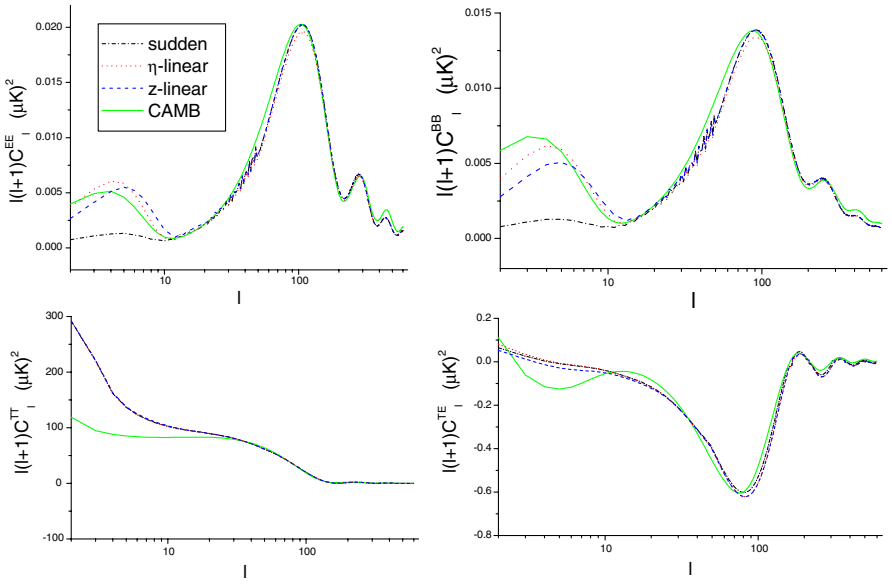

FIG. 8 (color online). The spectra C_l^{XX} in three reionization models. We take the parameters $c = 0.65$ and $b = 0.85$ in $D_r(k)$, as well as the optical depth $\kappa_r = 0.084$ and the ratio $r = 0.37$. The numerical result is obtained with the same set of parameters, using CAMB [16].

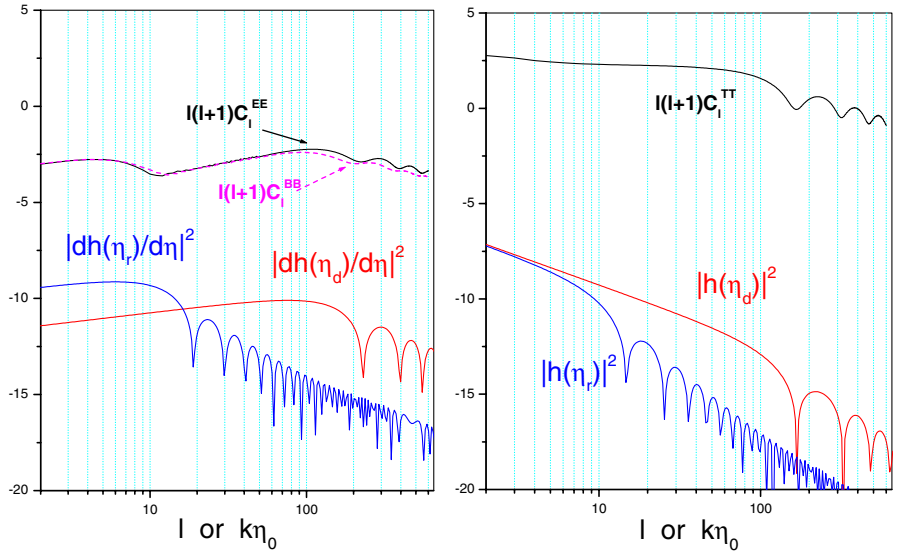

FIG. 9 (color online). The correspondence of the profiles of C_l^{XX} with that of RGWs at the decoupling and at the reionization. $\dot{h}(\eta_r)$ is responsible for the bumps of C_l^{EE} and C_l^{BB} around $l \sim 5$, while $\dot{h}(\eta_d)$ is responsible for the primary peaks and troughs for $l \geq 100$. For C_l^{TT}, $h(\eta_d)$ and $h(\eta_r)$ have a similar slope at $l \leq 10$, and their superposition does not form a prominent bump of C_l^{TT}.

can be further explained by the following analysis. The respective projection factors, P_{Tl}, P_{El}, and P_{Bl} as the integrands of C_l^{XX}, are made up of the spherical Bessel functions, $j_l(x)$, which are sharply peaked around $x \simeq l$. Subsequently, the projection factors as functions of k are sharply peaked around

$$k(\eta_0 - \eta_d) \simeq k\eta_0 \simeq l, \tag{72}$$

$$k(\eta_0 - \eta_r) \simeq l, \tag{73}$$

respectively. Consequently, the spectra as integrations over k will receive their main contributions from the integration range $k \sim l/\eta_0$ to the primary peaks and from $k \sim l/(\eta_0 - \eta_r)$ to the bump, respectively [33]:

$$C_l^{EE}, C_l^{BB} \propto A_1^2 D_d^2(k)|\dot{h}(\eta_d)|^2_{k\sim l/\eta_0} + A_2^2 D_r^2(k)|\dot{h}(\eta_r)|^2_{k\sim l/(\eta_0-\eta_r)}, \tag{74}$$

$$C_l^{TT} \propto e^{-2\kappa_r}|h(\eta_d)|^2_{k\sim l/\eta_0} + (1 - e^{-\kappa_r})^2|h(\eta_r)|^2_{k\sim l/(\eta_0-\eta_r)}, \tag{75}$$

$$C_l^{TE} \propto A_1 e^{-\kappa_r} D_d(k)h(\eta_d)\dot{h}(\eta_d)_{k\sim l/\eta_0} + A_2(1 - e^{-\kappa_r})D_r(k)h(\eta_r)\dot{h}(\eta_r)_{k\sim l/(\eta_0-\eta_r)}. \tag{76}$$

According to Eq. (74), the locations of the primary peaks of C_l^{EE} and C_l^{BB} are mainly determined by the $|\dot{h}(\eta_d)|^2$-term, and those of the reionization bumps are determined by the $|\dot{h}(\eta_r)|^2$-term. However, the spectrum C_l^{TT} does not have a prominent bump around $l \sim 5$. This is due to the fact that both $|h(\eta_d)|^2$ and $|h(\eta_r)|^2$ have a similar slope around there, and their superposition only enhances the spectral amplitude, not forming a bump. This is illustrated in Fig. 9.

2. The reionization bumps in the polarization spectra depend on the detailed reionization history. C_l^{EE} and C_l^{BB}, for a fixed value of the optical depth $\kappa_r = 0.084$ in the two extended models, are shown in Fig. 10. The bumps in the η-linear model are located at a slightly larger angular scale (smaller l) than those in the z-linear model. This is because we have assigned $\eta_r = 0.935$ in the η-linear model, which is greater than $\eta_r = 0.855$ in the z-linear model, so its bump is located at a slightly smaller $l \sim k(\eta_0 - \eta_r)$. Notice also that the η-linear model produces higher bumps than the z-linear model. This is due to the fact that the η-linear model has a greater width, $\Delta\eta_r = 0.286$, than that of the z-linear model, $\Delta\eta_r = 0.855$. Thus we conclude that the location of the bump is quite sensitive to the reionization time η_r, and the height of the bump is sensitive to the width $\Delta\eta_r$ of the reionization process. This feature is helpful for probing η_r and $\Delta\eta_r$ only if observational data on the bumps are accurate enough. However, when we let the two models have the same set of parameters, η_r and $\Delta\eta_r$, their reionization bumps predicted by our analytical formulation are very similar. The lesson here is that the bump is an integrating result from the ionization fraction $X_e(\eta)$, and, in this regard, two different reionization histories via $X_e(\eta)$ can lead to similar bumps, as long as they have similar $V_r(\eta)$ [63,64].

3. The overall profiles of CMB spectra are very sensitive to the optical depth κ_r of reionization. In particular, κ_r is strongly degenerate with the normalization of the amplitude of primordial fluctuations, and this fact has been one of the main difficulties in probing the details of the reionization process [9–13,65–67]. It should be emphasized

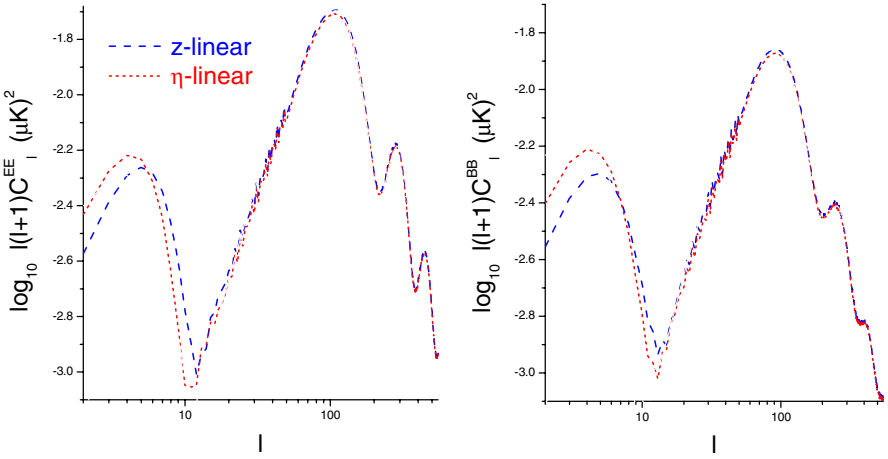

FIG. 10 (color online). C_l^{EE} and C_l^{BB} in the extended reionization models. The two models yield different reionization bumps at $l \sim 5$ since they are assigned different values of η_r and $\Delta\eta_r$.

that the reionization does not change the primordial amplitude A of RGWs in Eq. (6), which is implicitly contained in $h(\eta)$ and $\dot{h}(\eta)$. The impact of κ_r is through the coefficients $A_1(\kappa_r)$ and $A_2(\kappa_r)$ in β_l in Eq. (50), as well as the coefficients $e^{-\kappa_r}$ and $(1 - e^{-\kappa_r})$ in α_l in Eq. (58). The main features of the $\kappa_r - A$ degeneracy are clearly revealed by the analytical estimations in Eqs. (74)–(76).

For instance, look at C_l^{EE} and C_l^{BB} in Eq. (74). A larger κ_r gives smaller A_1 and larger A_2, leading to lower primary peaks and higher bumps of C_l^{EE} and C_l^{BB}, as illustrated in Fig. 11. But, this lowering of primary peaks can be compensated by the choice of a higher amplitude normalization A, which enhances the amplitude of $\dot{h}(\eta_d)$, resulting in the unchanged term $A_1^2(\kappa_r)|\dot{h}(\eta_d)|^2$, so that the primary peaks remain the same. This is the $\kappa_r - A$ degeneracy. Similar degeneracies in C_l^{TT} and C_l^{TE} are also understood from Eqs. (75) and (76).

The $\kappa_r - A$ degeneracy can be broken. Again, take C_l^{EE} and C_l^{BB} as examples. While a larger κ_r and a higher A can yield the unchanged primary peaks, the reionization bumps get doubly enhanced, since the bump term $A_2^2(\kappa_r)|\dot{h}(\eta_r)|^2$ in Eq. (74) gets doubly enhanced. This suggests a possible way to break the degeneracy. Equation (74) tells us that the relative height of the primary peaks and the bump is given by

$$\frac{\text{primary peak amplitude}}{\text{bump amplitude}} \propto \frac{A_1^2(\kappa_r)|\dot{h}(\eta_d)|^2}{A_2^2(\kappa_r)|\dot{h}(\eta_r)|^2}. \tag{77}$$

For any given RGWs, the ratio $|\dot{h}(\eta_d)|/|\dot{h}(\eta_r)|$ is independent of A and completely determined, so one has

$$\frac{\text{primary peak amplitude}}{\text{bump amplitude}} \propto \left(\frac{A_1(\kappa_r)}{A_2(\kappa_r)}\right)^2. \tag{78}$$

This ratio only depends on the value of κ_r and is not sensitive to the details of a reionization model. Therefore, using this ratio of heights, one can infer the value of κ_r from the observational data of C_l^{EE} and C_l^{BB}, thus breaking the degeneracy.

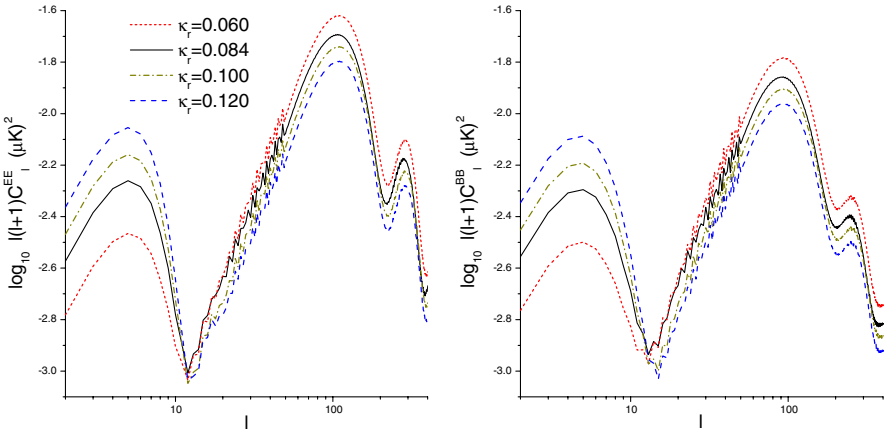

FIG. 11 (color online). The $\kappa_r - A$ degeneracy. A larger value of κ_r enhances the bumps at $l \sim 5$ and, at the same time, reduces the primary peaks of C_l^{EE} and C_l^{BB}. The plot is made for the z-linear model. This degeneracy behavior also exists in the η-linear model.

4. The primordial fluctuation spectral index $\beta_{\rm inf}$ introduced in Eq. (6) is a very important parameter for inflationary models. Given a normalization A of the RGW amplitude, a large $\beta_{\rm inf}$ tilts the spectrum $h(\nu, \eta_i)$ in such a way that the RGW is more strongly enhanced on smaller scales [38,39]. The RGW-generated spectra C_l^{XX} are subsequently tilted in the same way [33,34]. Therefore, a larger $\beta_{\rm inf}$ brings about an effect on C_l^{XX}, similar to what a smaller κ_r does, leading to certain bias in determining κ_r [67–71]. Take C_l^{EE} and C_l^{BB} as examples, for which the effect is more prominent. Figure 12 shows that, for the z-linear model, the bumps and primary peaks of the case ($\beta_{\rm inf} = -2.02$, $\kappa_r = 0.106$) almost overlap those of the case ($\beta_{\rm inf} = -2.10$, $\kappa_r = 0.084$), respectively.

The $\kappa_r - \beta_{\rm inf}$ degeneracy can also be understood by the analytical estimation in Eq. (74). While a large $\beta_{\rm inf}$ enhances $|\dot{h}(\eta_d)|^2$ on small scales, a large κ_r suppresses $A_1(\kappa_r)$, resulting in an unchanged combination $A_1(\kappa_r)^2|\dot{h}(\eta_d)|^2$ for the primary peaks. But this degeneracy is clearly broken from the second primary peak on. This is because the κ_r-induced change in $A_1(\kappa_r)$ is scale independent, whereas the $\beta_{\rm inf}$-induced change in $|h(\eta_d)|$ depends on the scale. Therefore, one expects that the data of the smaller scale C_l^{EE} and C_l^{BB} will be helpful in breaking the $\kappa_r - \beta_{\rm inf}$ degeneracy. Note also that the principal component method developed in Ref. [71] can protect the bias of κ_r caused by $\beta_{\rm inf}$.

5. Although the magnetic type of polarization C_l^{BB} is thought to be a "smoking gun" for the detection of RGWs, it has not been detected yet, which may be accomplished by a future CMBpol experiment [72]. The 5-year WMAP data [5,6] have given the observed cross spectrum C_l^{TE}, which is negative (anticorrelation) in a range $l \sim (50, 220)$. Yet this observed C_l^{TE} is a superposition of contributions by both scalar perturbations and RGWs. In order to extract the traces of RGWs out of C_l^{TE}, one still needs to disentangle the contribution by RGWs from the total. In the so-called zero-multipole method [27,45,73,74], one examines the impact of the tensor/scalar ratio r upon the zero multipole l_0 around ~50, where C_l^{TE} first crosses the value 0 and then turns negative. However, there are other factors that can influence the value of l_0. The variation of l_0 caused by NFS has been estimated to be small, $\Delta l \leq 4$ [34]. Here the reionization is another important factor that brings about a change of l_0, as is shown in Fig. 13 for the extended reionization models with $\kappa_r = 0.084$. Around the relevant region of $l \sim 50$, the reionization shifts the curve of C_l^{TE} to smaller angular scales by an amount of $\Delta l \sim 20$, in comparison with the nonreionized C_l^{TE}. This amount is much larger than that caused by NFS. Moreover, the shift Δl increases with the optical depth κ_r. This significant effect has to be incorporated into the zero-multipole analysis before one can make an extraction of RGWs from the total C_l^{TE}.

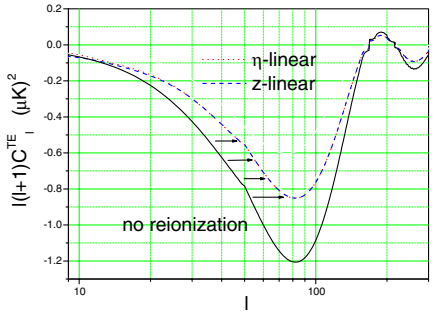

FIG. 13 (color online). Reionization shifts C_l^{TE} to smaller angular scales by $\Delta l \sim 20$ around the region $l \sim 50$. For illustration purposes, we take $\kappa_r = 0.084$ and $r = 0.37$.

In this procedure, besides disentangling the adiabatic (constant entropy) modes that are dominant in the scalar perturbations, one needs to consider the isocurvature modes possibly existing in the cosmological plasma [75], which can contribute to C_l^{XX} [76]. In particular, the isocurvature modes contribute positively (correlation) to the cross spectrum C_l^{TE} in the range around $l \sim 100$, in contrast to the adiabatic modes, which contribute negatively

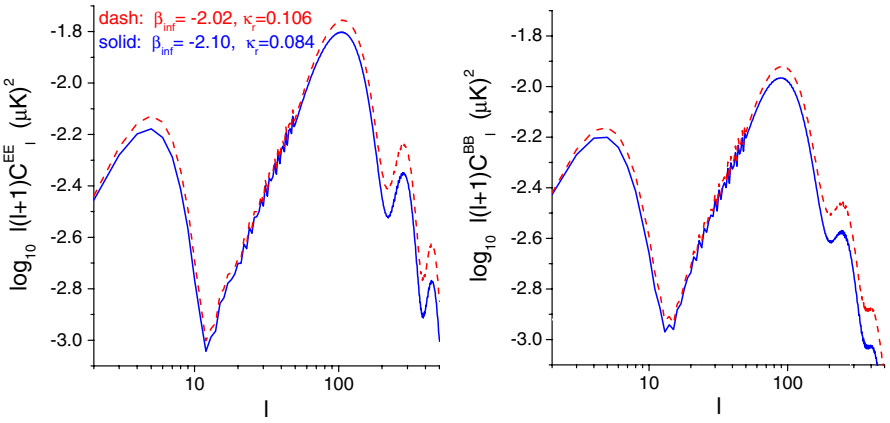

FIG. 12 (color online). The $\kappa_r - \beta_{\rm inf}$ degeneracy. Although the bumps and the first primary peaks are degenerate, the second and third primary peaks show a clear departure. The plot is made for the z-linear model.

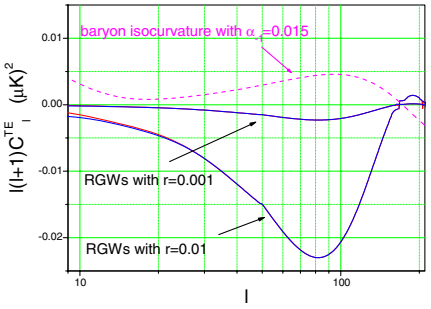

FIG. 14 (color online). C_l^{TE} from the baryon isocurvature mode is positive around $l \sim 100$, whereas that from RGWs is negative there. Only when a very small $r = 0.001$ is taken can the amplitude of C_l^{TE} from the isocurvature modes be comparable to that from RGWs. The C_l^{TE} from the isocurvature modes is the numerical result generated using CAMB [16], with $\alpha_{-1} = 0.015$.

(anticorrelation) there. The observed C_l^{TE} from WMAP has shown the anticorrelation, and a very stringent constraint has been found on the isocurvature contribution with the isocurvature/adiabatic ratio $\alpha_{-1} < 0.015$ at 95% CL [5]. It is interesting to compare the contributions from RGWs and isocurvature perturbations to C_l^{TE}. The comparison is very sensitive to the ratio α_{-1} and the tensor/scalar ratio r. Taking the upper limit $\alpha_{-1} = 0.015$ constrained from WMAP-5, and using the CAMB online tool [16] results for isocurvature modes of the plasma components of baryons, CDM, and neutrinos, one finds that when $r = 0.37$ is taken, the amplitude of C_l^{TE} generated by RGWs is about 2 orders greater than that of the isocurvature modes. So in this case the isocurvature can be neglected. Only when a much smaller ratio $r = 0.001$ is taken can the contribution by the isocurvature modes be comparable to that by RGWs. This is demonstrated with $r = 0.001$ and $r = 0.01$ in Fig. 14, in which the numerical C_l^{TE} contributed by the baryon isocurvature perturbation has been produced by CAMB [16] with $\alpha_{-1} = 0.015$.

6. So far, our analytic formulation for reionization can only distinguish two different extended models by comparing their κ_r, η_r, and $\Delta\eta_r$. The damping factor $D_r(k)$ in Eq. (46) as a fitting formula could be used to specify other fine details of two reionization models. Obviously, with a fixed b, a larger c leads to lower bumps of C_l^{EE} and C_l^{BB}, as shown in Fig. 15 for the z-linear model. On the other hand, with a fixed c, a larger b will yield slightly higher reionization bumps, while leaving the primary peaks almost intact. This property can be inferred as follows. For the reionization bump around $l \sim 5$, the contribution is mainly from $k \sim l/(\eta_0 - \eta_r)$ according to Eq. (73), so $D_r(k) \propto e^{-c(\Delta\eta_r l/(\eta_0-\eta_r))^b}$. In the reionization models considered in this paper, the combination $\Delta\eta_r l/(\eta_0 - \eta_r) \sim 0.5 < 1$, so a larger parameter b leads to a larger D_r and higher bumps. For the primary peaks with $l \geq 100$, $D_r(k)$ is so small that the term $A_2^2 D_r^2(k)|\dot{h}(\eta_r)|^2_{k\sim l/(\eta_0-\eta_r)}$ to C_l^{EE} and C_l^{BB} is practically negligible, leaving the primary peaks intact under a variation of b in $D_r(k)$.

VI. SUMMARY

We have presented the approximate, analytical formulation of the reionized CMB spectra C_l^{XX} generated by RGWs. Even though it is an approximation and serves as a complement to the numerical codes, it does improve our understanding CMB and efficiently promote the analysis of various effects that reionization brings upon C_l^{XX}.

The reionization around $z \sim 11$ is studied using three simple homogeneous models, i.e., a sudden reionization, and two extended reionizations with ionization fractions $X_e(\eta) \propto \eta$ and $X_e(\eta) \propto z$. The key parameter is κ_r, the optical depth from the present to the start of reionization. Given a value of κ_r in each model, the visibility function $V_r(\eta)$ follows, which is approximately fitted by Gaussian-type functions. This procedure is similar to the treatment of decoupling in our previous study.

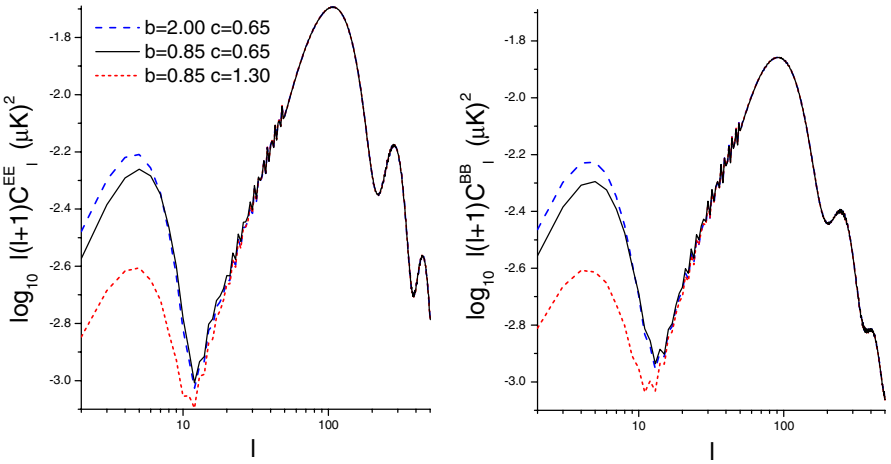

FIG. 15 (color online). The damping factor $D_r(k)$ in Eq. (46) depends on the parameters c and b. The plot is made for the z-linear model.

Then the time integrations for the polarization mode β_l and the temperature anisotropy mode α_l are carried out approximately, and the resulting analytic expressions consist of contributions from the RGWs $h(\eta_d)$ and $\dot{h}(\eta_d)$ at the decoupling, and from $h(\eta_r)$ and $\dot{h}(\eta_r)$ at the reionization as well. It is found that, while $h(\eta_d)$ and $\dot{h}(\eta_d)$ generate primary peaks at $l \geq 100$, $\dot{h}(\eta_r)$ produces bumps for C_l^{EE} and C_l^{BB} at $l \sim 5$, and $h(\eta_r)$ enhances C_l^{TT} and C_l^{TE} there. The analytic C_l^{XX} qualitatively agree with those computed numerically, such as by CAMB.

As a merit of our analytic approach, the dependence of C_l^{XX} upon the optical depth κ_r is explicitly given, in terms of the coefficients $a_1(\kappa_r)$ and $a_2(\kappa_r)$ for the polarization $\beta_l(\eta_0)$, and of the coefficients $e^{-\kappa_r}$ and $(1 - e^{-\kappa_r})$ for the temperature anisotropies $\alpha_l(\eta_0)$. It is found that $a_1(\kappa_r)$ and $a_2(\kappa_r)$ vary with κ_r more quickly than $e^{-\kappa_r}$ and $(1 - e^{-\kappa_r})$, respectively. Therefore, the polarization β_l is more sensitive to κ_r than the temperature anisotropies α_l. A larger κ_r gives higher $a_2(\kappa_r)$ and lower $a_1(\kappa_r)$; i.e., it yields higher bumps and lower primary peaks in C_l^{EE} and C_l^{BB}. Thus there is a degeneracy of κ_r with the normalization of the initial amplitude A of RGWs. Besides, κ_r also has a weak degeneracy with the spectral index $\beta_{\rm inf}$ of RGWs since a larger $\beta_{\rm inf}$ enhances the primary peaks on small scales. The analytical C_l^{EE} and C_l^{BB} also suggest possible ways to break these two kinds of degeneracies.

Besides κ_r, our formulation also demonstrates the effects of the reionization time η_r and the reionization duration $\Delta\eta_r$. For a fixed κ_r, the height of the bump is proportional to $\Delta\eta_r$, and the location l of the bump depends on η_r in such a way, $l \sim k(\eta_0 - \eta_r)$, that a later reionization (larger η_r) yields a bump at larger angular scales (smaller l).

Given a fixed set of parameters, κ_r, η_r, and $\Delta\eta_r$, the η-linear and z-linear models yield similar bumps in C_l^{EE} and C_l^{BB}. Thus, our analytical formulation is unable to rediscover the reionization history $X_e(\eta)$ from C_l^{XX}.

These analytical results tell us that studying the reionization by means of CMB temperature anisotropies and polarization not only requires sufficient observational data, but also needs detailed research of the reionization process itself and more realistic modeling.

The reionization process also significantly affects the possible detection of RGWs via the observations of C_l^{XX}. In particular, it is found that the reionization causes a shift of the zero multipole l_0 of the cross spectrum C_l^{TE} by a substantial amount, $\Delta l \sim 20$, which is also κ_r dependent. The effect of reionization needs to be properly included before one can apply the zero-multipole method to extract the traces of RGWs from the observed C_l^{TE}.

ACKNOWLEDGMENTS

T. Y. Xia's work has been partially supported by Graduate Student Research Funding from USTC. Y. Zhang's research has been supported by the CNSF Grant No. 10773009, SRFDP, and CAS. We thank Dr. W. Zhao for interesting discussions.

[1] D. N. Spergel *et al.*, Astrophys. J. Suppl. Ser. **148**, 175 (2003).
[2] H. V. Peiris *et al.*, Astrophys. J. Suppl. Ser. **148**, 213 (2003).
[3] D. N. Spergel *et al.*, Astrophys. J. Suppl. Ser. **170**, 377 (2007).
[4] L. Page *et al.*, Astrophys. J. Suppl. Ser. **170**, 335 (2007).
[5] E. Komatsu *et al.*, Astrophys. J. Suppl. Ser. **180**, 330 (2009).
[6] M. R. Nolta *et al.*, Astrophys. J. Suppl. Ser. **180**, 296 (2009).
[7] G. Hinshaw *et al.*, arXiv:0803.0732.
[8] J. Dunkley *et al.*, Astrophys. J. Suppl. Ser. **180**, 306 (2009).
[9] M. Zaldarriaga, Phys. Rev. D **55**, 1822 (1997).
[10] M. Zaldarriaga, D. Spergel, and U. Seljak, Astrophys. J. **488**, 1 (1997).
[11] M. Zaldarriaga and U. Seljak, Phys. Rev. D **55**, 1830 (1997).
[12] A. Venkatesan, Astrophys. J. **537**, 55 (2000).
[13] A. Venkatesan, Astrophys. J. **572**, 15 (2002).
[14] K. L. Ng and K. W. Ng, Astrophys. J. **456**, 413 (1996).
[15] U. Seljak and M. Zaldarriaga, Astrophys. J. **469**, 437 (1996).
[16] A. Lewis, A. Challinor, and A. Lasenby, Astrophys. J. **538**, 473 (2000); the CAMB online tool is located at http://lambda.gsfc.nasa.gov/toolbox/tb_camb_form.cfm.
[17] S. Sasaki, Prog. Theor. Phys. **76**, 1036 (1986).
[18] V. F. Mukhanov, H. A. Feldman, and R. H. Brandenberger, Phys. Rep. **215**, 203 (1992).
[19] W. Hu and N. Sugiyama, Astrophys. J. **444**, 489 (1995).
[20] M. M. Basko and A. G. Polnarev, Mon. Not. R. Astron. Soc. **191**, 207 (1980).
[21] A. Polnarev, Sov. Astron. **29**, 607 (1985).
[22] R. Crittenden, D. Coulson, and N. G. Turok, Phys. Rev. D **52**, R5402 (1995).
[23] R. K. Sachs and Q. M. Wolfe, Astrophys. J. **147**, 73 (1967).
[24] U. Seljak and M. Zaldarriaga, Phys. Rev. Lett. **78**, 2054 (1997).
[25] M. Kamionkowski, A. Kosowsky, and A. Stebbins, Phys. Rev. D **55**, 7368 (1997).
[26] B. Keating, P. Timbie, A. Polnarev, and J. Steinberger, Astrophys. J. **495**, 580 (1998).

[27] B. Keating, A. Polnarev, N. Miller, and D. Baskaran, Int. J. Mod. Phys. A **21**, 2459 (2006).
[28] A. Kosowsky, Ann. Phys. (N.Y.) **246**, 49 (1996).
[29] M. Zaldarriaga and D. Harari, Phys. Rev. D **52**, 3276 (1995).
[30] L. Grishchuk, Phys. Rev. D **48**, 3513 (1993); Phys. Rev. Lett. **70**, 2371 (1993); arXiv:0707.3319.
[31] W. Zhao, D. Baskaran, and L. P. Grishchuk, Phys. Rev. D **79**, 023002 (2009).
[32] J. Pritchard and M. Kamionkowski, Ann. Phys. (N.Y.) **318**, 2 (2005).
[33] W. Zhao and Y. Zhang, Phys. Rev. D **74**, 083006 (2006).
[34] T. Y. Xia and Y. Zhang, Phys. Rev. D **78**, 123005 (2008).
[35] S. Weinberg, Phys. Rev. D **69**, 023503 (2004).
[36] D. A. Dicus and W. W. Repko, Phys. Rev. D **72**, 088302 (2005).
[37] Y. Watanabe and E. Komatsu, Phys. Rev. D **73**, 123515 (2006).
[38] H. X. Miao and Y. Zhang, Phys. Rev. D **75**, 104009 (2007).
[39] Y. Zhang *et al.*, Classical Quantum Gravity **22**, 1383 (2005); **23**, 3783 (2006); Int. J. Mod. Phys. D **17**, 1105 (2008).
[40] S. Wang, Y. Zhang, T. Y. Xia, and H. X. Miao, Phys. Rev. D **77**, 104016 (2008).
[41] D. J. Schwarz, Mod. Phys. Lett. A **13**, 2771 (1998).
[42] L. Grishchuk, Lect. Notes Phys. **562**, 167 (2001).
[43] A. R. Liddle and D. H. Lyth, Phys. Lett. B **291**, 391 (1992).
[44] L. Verde *et al.*, Astrophys. J. Suppl. Ser. **148**, 195 (2003).
[45] D. Baskaran, L. P. Grishchuk, and A. G. Polnarev, Phys. Rev. D **74**, 083008 (2006).
[46] Y. Cen, Astrophys. J. **591**, 12 (2003).
[47] T. Giannantonio and R. Crittenden, Mon. Not. R. Astron. Soc. **381**, 819 (2007).
[48] L. P. L. Colombo *et al.*, Astron. Astrophys. **435**, 413 (2005).
[49] P. J. E. Peebles, Astrophys. J. **153**, 1 (1968).
[50] B. J. T. Jones and R. F. G. Wyse, Astron. Astrophys. **149**, 144 (1985).
[51] A. J. Benson, A. Nusser, N. Sugiyama, and C. G. Lacey, Mon. Not. R. Astron. Soc. **320**, 153 (2001).
[52] G. C. Liu *et al.*, Astrophys. J. **561**, 504 (2001).
[53] M. Santos *et al.*, Astrophys. J. **598**, 756 (2003).
[54] J. Zhang, L. Hui, and Z. Haiman, Mon. Not. R. Astron. Soc. **375**, 324 (2007).
[55] M. Mortonson and W. Hu, Astrophys. J. **657**, 1 (2007).
[56] P. Naselsky and L. Y. Chiang, Mon. Not. R. Astron. Soc. **347**, 795 (2004).
[57] S. Furlanetto and A. Loeb, Astrophys. J. **634**, 1 (2005).
[58] L. Hui and Z. Haiman, Astrophys. J. **596**, 9 (2003).
[59] X. H. Fan, C. L. Carilli, and B. Keating, Annu. Rev. Astron. Astrophys. **44**, 415 (2006); X. Fan *et al.*, Astron. J. **132**, 117 (2006).
[60] P. J. E. Peebles, *Principles of Physical Cosmology* (Princeton University Press, Princeton, 1993).
[61] R. Trotta and S. Hansen, Phys. Rev. D **69**, 023509 (2004).
[62] L. M. Griffiths, D. Barbosa, and A. R. Liddle, Mon. Not. R. Astron. Soc. **308**, 854 (1999).
[63] L. P. L. Colombo, J. Cosmol. Astropart. Phys. 03 (2004) 003.
[64] P. Mukherjee and A. R. Liddle, Mon. Not. R. Astron. Soc. **389**, 231 (2008).
[65] L. M. Griffiths and A. R. Liddle, Mon. Not. R. Astron. Soc. **324**, 769 (2001).
[66] M. Kaplinghat *et al.*, Astrophys. J. **583**, 24 (2003).
[67] L. P. L. Colombo and E. Pierpaoli, New Astron. **14**, 269 (2009).
[68] G. Jungman, M. Kaminokowski, A. Kosowsky, and D. N. Spergel, Phys. Rev. D **54**, 1332 (1996).
[69] E. J. Eisenstein, W. Hu, and M. Tegmark, Astrophys. J. **518**, 2 (1999).
[70] L. P. L. Colombo and S. A. Bonometto, New Astron. **8**, 313 (2003).
[71] M. J. Mortonson and W. Hu, Phys. Rev. D **77**, 043506 (2008).
[72] D. Baumann *et al.*, arXiv:0811.3919; arXiv:0811.3911; M. Zaldarriaga *et al.*, arXiv:0811.3918.
[73] A. G. Polnarev, N. J. Miller, and B. G. Keating, Mon. Not. R. Astron. Soc. **386**, 1053 (2008).
[74] N. J. Miller, B. G. Keating, and A. G. Polnarev, Adv. Astron. Astrophys. 09 (**2009**) 309024.
[75] M. Bucher, K. Moodley, and N. Turok, Phys. Rev. D **62**, 083508 (2000); Phys. Rev. Lett. **87**, 191301 (2001).
[76] K. Enqvist, H. Kurki-Suonio, and J. Valiviita, Phys. Rev. D **62**, 103003 (2000); K. Enqvist and H. Kurki-Suonio, Phys. Rev. D **61**, 043002 (2000).